The Calculation of Spectroscopic Jahn−Teller Parameters by *ab Initio* Methods

Timothy A. Barckholtz and Terry A. Miller*

Laser Spectroscopy Facility, Department of Chemistry, The Ohio State University, 120 West 18th Avenue, Columbus, Ohio 43210-1173

Received: September 23, 1998; In Final Form: November 25, 1998

We report a general method for the calculation of Jahn−Teller coupling constants by *ab initio* methods widely available today in standard packages. The vibrational frequencies corresponding to those obtained experimentally are calculated at the symmetric position using a generalized restricted Hartree−Fock (GRHF) wavefunction. The energy of the symmetric configuration is calculated as a conical intersection using a complete active space self-consistent field (CASSCF) wavefunction. The energy of the distorted configuration is calculated using the same CASSCF active space and occupations. The difference in energy of these two CASSCF calculations is the Jahn−Teller stabilization energy. In addition to the total energy of the state at the cusp, the conical intersection calculation determines the vector along which the molecule will distort. This vector is projected onto the normal modes of the molecule, obtained via the GRHF calculation, so that estimates of the experimentally observable linear Jahn−Teller coupling constants can be obtained. We also present a method for the calculation of the quadratic Jahn−Teller coupling constants. This approach has been applied to and evaluated for the methoxy family of radicals (CH_3O, CF_3O, CH_3S, and CF_3S).

1. Introduction

The Jahn−Teller effect[1]—that a nonlinear molecule in an orbitally degenerate state will spontaneously distort from a symmetric to an asymmetric configuration—is one of the most fascinating phenomena in chemistry. Jahn−Teller coupling has been observed in a wide variety of systems, including fullerenes,[2] octahedral transition metal complexes,[3] solid-state physics and chemistry,[4−6] and gas phase radicals[7] and ions.[8] Jahn−Teller coupling has even been suggested as the cause for the anomalous heat release in "cold fusion".[9] The recent blossoming of the field of femtochemistry has given rise to numerous studies of the expected dynamics of Jahn−Teller active molecules.[10]

Historically, most of the experimental research on Jahn−Teller active molecules has been done in condensed or solid phases, precluding the possibility of obtaining detailed experimental information about the potential energy surfaces (PES). However, recently a number of investigations on isolated, gas-phase Jahn−Teller active radicals and ions have been performed that do provide detailed information about the Jahn−Teller surfaces. The combination of laser spectroscopy and free jet expansions[11] has been applied to obtain the vibronic structure, and in some cases the rotational structure, of the methoxy family of radicals (CH_3O,[12−16] CH_3S,[13,17] CF_3O,[18] and CF_3S[19,20]), the cyclopentadienyl radical,[21] the benzene cation,[22] the halogen-substituted benzene cations,[8,23,24] the excited states of ammonia,[25] the excited states of H_3,[26] and the ground and excited states of the alkali and coinage metal trimers M_3 (M = Na,[27] Cu,[28] Ag[30]). The precision of these experiments provides an ideal benchmark for the evaluation of *ab initio* methods for Jahn−Teller surfaces.

It is generally known that Jahn−Teller coupling distorts the geometry of the molecule such that the minimum of the PES is not at the symmetric configuration of the nuclei, but at an asymmetric configuration. What is less generally known is the effect Jahn−Teller coupling has on the experimentally observable vibrational energy levels of the state. While Jahn−Teller coupling may distort the bond lengths by less than 0.1 Å or bond angles by less than 1°, the same amount of Jahn−Teller coupling might shift and/or split the vibrational energy levels by hundreds of cm^{-1}. Very significant effects may be seen in the spin−orbit splittings as well as in the rotational structure.

Many quantum chemical calculations have been performed in order to determine the distorted geometry and total energy of Jahn−Teller molecules, a partial list of which includes organic, cyclic π systems[31,32] (C_3H_3,[33] $C_4H_4^+$,[34] C_5H_5,[35] $C_6H_6^+$,[36−39] $C_6H_6^-$,[39,40] $C_6F_6^+$,[36] C_7H_7,[41] and $C_8H_8^+$ [42]), trimethylenemethane,[43] the methane cation and its derivatives (CH_4^+,[44−46] CF_4^+,[47] CCl_4^+,[48] and the heavier ions[49]), the ammonium radical (NH_4),[50] the methoxy[51,52] and trifluoromethoxy[53] radicals, and several small transition metal complexes.[31,54,55] There have been far fewer attempts aimed at the calculation of the experimentally observable vibronic coupling constants that characterize the geometric distortion, vibrational shifts and splittings, and rotational structure. This is particularly important, since it is just such calculations that would be of the most aid in the spectral analysis. Conversely, experimental results should be used to judge the quality of a particular calculation.

Quantum chemistry has rapidly progressed to the point where standard *ab initio* calculations can predict many spectroscopic parameters of closed-shell molecules and states to reasonably good accuracy. Bond lengths and angles for organic molecules can be typically calculated to within a few percent of the experimental values,[56] which means that the rotational constants can be calculated to comparable accuracy. Vibrational frequencies can be calculated to within 50 cm^{-1},[57] a reasonably good level of accuracy. Many thermodynamic properties of small organic molecules can be calculated to within a few kcal/mol accuracy using the G1,[58] G2,[59] G2MP2,[60] and complete basis set[61] methodologies. With the development of methods that include high levels of electron correlation (and the development of computers to run these calculations), even properties such

10.1021/jp983829x CCC: $18.00
Published on Web 01/22/1999

as the binding energy in van der Waals complexes can be calculated accurately.[62]

However, no method has yet been reported to accurately and systematically calculate the vibronic parameters that are used to experimentally characterize a Jahn−Teller active molecule. In this paper, we initiate efforts to rectify this situation. We present a method to calculate the vibrational frequencies of a Jahn−Teller molecule, both those of the active and of the inactive modes. For the active modes, these frequencies correspond to those of the undistorted molecule, which are the values available from a standard Jahn−Teller analysis of an experimental spectrum. Our method also predicts the experimentally measurable linear and quadratic Jahn−Teller coupling constants as well as the resultant stabilization energies and distorted geometries. One clear advantage of our method is that it relies exclusively on *ab initio* programs that are widely available today in commercial packages.

Our calculations are designed to serve several purposes. First, the extremely detailed experiments that have been performed on the isolated methoxy radicals, and to a lesser extent the Jahn−Teller active aromatic systems, serve as benchmarks against which the *ab initio* calculations can be compared. If an *ab initio* calculation is validated, it likely will supply additional information (e.g., detailed geometries, thermodynamic properties, etc.) about the molecule that is not readily obtained experimentally. Second, the spectra of Jahn−Teller molecules are often quite complex and difficult to analyze. Therefore, an *ab initio* method that can predict the constants used in a Jahn−Teller analysis is extremely valuable to the experimentalist, even if its precision is limited. Even a qualitatively correct prediction of the energy levels or simulated spectrum would be of significant value to the experimentalist trying to analyze exceedingly complex experimental data. To accomplish these tasks, we will clarify what should and should not be inferred from a given *ab initio* calculation for a Jahn−Teller molecule and how the results relate to experimental observables.

We first present a condensed version of the quantum mechanics of a Jahn−Teller state, with particular emphasis on the geometry of the PES and the resultant parameters that are used in the spectroscopic analysis of the vibronic energy levels. We then outline the goals of an *ab initio* calculation on a Jahn−Teller molecule, review previous work in this area, and present our approach. The methoxy family radicals are used to evaluate how well the calculations perform.

2. The Jahn−Teller Potential Energy Surface

It is instructive to review the general shape and character of the PES of a Jahn−Teller active molecule.[63−68] The Jahn−Teller PES is a special case of a crossing between two electronic states. Curve crossings have been intensely researched for nearly three-quarters of a century,[69] yet much still remains to be learned about them. A number of excellent expositions on this topic have appeared in the literature, and we refer the reader to them for discussion of many of the details that we will forego here.[70−75]

There are several types of curve crossings that might occur for a nonlinear molecule. The most familiar type is the "accidental" crossing of two or more electronic states. These crossings occur not because of symmetry constraints but merely because the energies of the two states "accidentally" become coincident at the geometry of the crossing. This type of curve crossing is extremely important in the photochemistry of molecules, mostly because the density of excited electronic states is generally quite high in the neighborhood of ultraviolet excitation energies.[71]

The Jahn−Teller PES is a special case of a curve crossing for a molecule that nominally belongs to a point group with a C_3 or higher axis. A Jahn−Teller distortion occurs when the electronic state is orbitally degenerate, for example, a ^{2}E state of a C_{3v} molecule. In this case, a "curve crossing" occurs at the symmetric configuration of the nuclei between the two components of the degenerate electronic state (Figure 1a−c illustrates the normal spectroscopic interpretation of the Jahn−Teller distorted PES). At the symmetric configuration, $\mathbf{X}_0$, the gradient of the potential with respect to some of the vibrational degrees of freedom is nonzero. This gives rise to linear Jahn−Teller coupling, whereby a distortion along the vibrational coordinates of an appropriate symmetry will lift the degeneracy and stabilize the molecule. If cylindrical coordinates ρ_i and ϕ_i are used to describe the vibrational coordinates of the Jahn−Teller active mode, a moat of minimum energy is found at $\rho_{\min}$.[76] In the absence of quadratic Jahn−Teller coupling, the PES is a constant for all values of ϕ_i at $\rho_{\min}$ and the molecule is free to "pseudorotate" about the moat (Figure 1b). However, if quadratic Jahn−Teller coupling cannot be neglected, local minima ($E_{\min,i}$) and maxima ($E_{\max,i}$) exist about the moat, giving rise to at least partially hindered pseudorotation (Figure 1c).

A useful distinction is often made between a "static" Jahn−Teller effect and a "dynamic" Jahn−Teller effect. The former refers to the situation when the Jahn−Teller coupling is sufficiently strong to permanently distort the molecule. In this case, a Hamiltonian appropriate for the point group of the distorted molecule is most suitable for the analysis of the vibronic and rotational structure. The dynamic Jahn−Teller effect[77] occurs when the molecule is not localized at the geometry of the global minimum in the potential energy surface at the distorted configuration. In this case, a Hamiltonian of the symmetric molecule is most often used, with several corrections added to it to account for the slight distortion of the PES. In this paper, we will be concerned only with dynamic Jahn−Teller coupling.

While not necessarily a curve crossing *per se*, "pseudo-Jahn−Teller coupling" is, as the name implies, closely related to Jahn−Teller coupling.[78] The pseudo-Jahn−Teller effect occurs when one electronic state is mixed with another via vibronic coupling. In this case, neither a curve crossing nor a degenerate electronic state is required. Pseudo-Jahn−Teller coupling is strongest between states close in energy, such as occurs between the ^{1}A$_1'$ and ^{1}E$'$ states derived from an $(e'')^2$ configuration of a D_{3h} molecule. We will not discuss pseudo-Jahn−Teller coupling or "accidental" curve crossings any further, rather we restrict ourselves to "true" Jahn−Teller crossings.

Parts a′−c′ of Figure 1 represent *different* slices through the *same* PES as in Figure 1a−c. The primed slices are the planes that contain the points $\mathbf{X}_0$, $\mathbf{X}_{\max}$, and $\mathbf{X}_{\min}$. These points correspond respectively to the symmetrical configuration of the nuclei and the configurations at which there is the minimum of energy, $E_{\min}$, and its local maximum, $E_{\max}$. (In (b′) $E_{\min} = E_{\max}$.) Since the primed figures require $\mathbf{X}_{\max}$ and $\mathbf{X}_{\min}$, which are known only from calculations, the lower set of slices in Figure 1 is most important for our *ab initio* calculations. A key purpose of this paper will be to relate this lower set of traces of Figure 1 to the experimentally accessible upper set.

The Jahn−Teller PES contains several unique features that cause complications in both the spectroscopy of the state and in *ab initio* calculations of it. First, the symmetric configuration, which is used as the basis for the spectroscopic analyses, is a conical intersection of the two components of the electronic

TABLE 1: Terms in the Vibronic Jahn−Teller Potential[a]

term	description	form
$\hat{H}_e^0$	electronic potential at the symmetric configuration	Coulomb, exchange, ...
$\hat{H}_{h,a_1}$	harmonic oscillator for the modes that are not Jahn−Teller active	$\sum_{i=1}^{3N-6-2p} \frac{1}{2}\lambda_i \lvert Q_i\rvert^2$
$\hat{H}_{h,e}$	harmonic oscillator for the p Jahn−Teller active mode	$\sum_{i=1}^{p}\sum_{r=+,-} \frac{1}{2}\lambda_i \lvert Q_{i,r}\rvert^2$
$\hat{H}_l$	linear Jahn−Teller coupling	$\sum_{i=1}^{p}\sum_{r=+,-} k_i Q_{i,r}$
$\hat{H}_{q_{ii}}$	quadratic Jahn−Teller coupling within a single mode	$\sum_{i=1}^{p}\sum_{r=+,-} \frac{1}{2}g_{ii}(Q_{i,r})^2$
$\hat{H}_{q_{ij}}$	quadratic Jahn−Teller coupling between two modes	$\sum_{i=1}^{p}\sum_{r=+,-}\sum_{j>i} \frac{1}{2}g_{ij}Q_{i,r}Q_{j,r}$

[a] The parameters are defined as

$$\lambda_i = \left\langle E_\pm \middle| \left(\frac{\partial^2 \hat{V}}{\partial Q_{i,+}\partial Q_{i,-}}\right)_0 \middle| E_\pm \right\rangle; \qquad k_i = \left\langle E_\pm \middle| \left(\frac{\partial \hat{V}}{\partial Q_{i,\pm}}\right)_0 \middle| E_\mp \right\rangle; g_{ij} = \left\langle E_\pm \middle| \left(\frac{\partial^2 \hat{V}}{\partial Q_{i,\pm}\partial Q_{j,\pm}}\right)_0 \middle| E_\mp \right\rangle$$

with $Q_{i,\pm} = \rho_i e^{\pm i\phi_i}$.

state. Only recently have *ab initio* methods been developed to handle this situation properly.[70,74,79−82] Furthermore, the first derivatives at the conical intersection are nonzero, making calculations of the vibrational normal modes and frequencies at this point difficult. However, as we show in the next section, it is precisely these normal modes and frequencies that are used as the starting point for the spectroscopic analysis of the vibronic structure of the state.

3. Summary of the Jahn−Teller Effect in Spectroscopy

The Jahn−Teller theorem is applicable to orbitally degenerate states, which necessitate open-shell electronic configurations. All of the Jahn−Teller molecules that we will discuss have doublet spin states, though vibrationally resolved spectra have been obtained for a few Jahn−Teller active molecules in other spin states. In the following discussion, we restrict ourselves to a ^{2}E state of a molecule belonging to the C_{3v} point group, which is appropriate for the ground states of the methoxy radicals, which we use as examples. Others have presented analagous derivations for the other point groups, including those with a C_4 principal axis[83−85] and the cubic point groups.[86,87]

Jahn−Teller coupling causes a breakdown of the Born−Oppenheimer approximation, which means that the nuclear and electronic degrees of freedom cannot be conveniently separated, as is the case for most molecules. The consequence of this breakdown for spectroscopy and *ab initio* calculations is that defining a PES, a Hamiltonian, and a basis set is not a trivial matter. Nearly all analyses of the vibronic structure of Jahn−Teller states have used as the reference or zeroth-order wavefunction the eigenfunctions of the harmonic oscillator Hamiltonian of the *undistorted* molecule. This might seem like an odd choice, considering that the undistorted molecule is not a minimum on the PES. However, it is a very convenient choice, as corrections to the Hamiltonian can be evaluated in terms of the harmonic oscillator basis functions. The alternative is to start with a harmonic oscillator Hamiltonian and basis set for the distorted molecule. Corrections to this Hamiltonian must still be added, as the PES is not harmonic, nor can it be readily approximated *via* anharmonic corrections. To the best of our knowledge, no one has yet gone this route in analyzing the vibronic structure of Jahn−Teller states. An additional advantage of starting with the undistorted molecule as the reference state is that it provides a clear and simple way to include spin−orbit coupling in calculations of the spin-vibronic structure.[19]

For these reasons, we take as the starting point for the spectroscopic analyses of the vibrational and rotational structure of Jahn−Teller states the harmonic oscillator and symmetric top basis functions appropriate for the symmetric configuration of the nuclei. At the symmetric configuration of the nuclei, the electronic wavefunction is degenerate and the two (complex) components, $E_\pm$, of the ^{2}E electronic wavefunction can be labeled by $\Lambda = \pm 1$. To the electronic basis set we append the harmonic oscillator basis functions for the p two-dimensional Jahn−Teller active modes and the $3N - 6 - 2p$ harmonic oscillator basis functions for the non-Jahn−Teller active modes. For the methoxy family of radicals, all of which belong to the C_{3v} point group, these basis functions are of e and a_1 symmetry, respectively. (There are no vibrational modes of a_2 symmetry in the methoxy radical.) To include spin−orbit coupling in the calculation, the projection, Σ, of **S** on the symmetry axis is also appended to the basis set.

The vibration−rotation Hamiltonian for a Jahn−Teller state has been derived in detail elsewhere,[19] and we will only present the results of the derivations here, which will serve to define the molecular parameters that are obtained from the spectral analyses and *ab initio* calculations. The Hamiltonian for the molecule is the sum of a number of terms,

$$\hat{H} = \hat{H}_T + \hat{V} + \hat{H}_{SO} + \hat{H}_{rot} \tag{1}$$

where $\hat{H}_T$ is the kinetic energy of the nuclei. The potential energy, $\hat{V}$, is a function of the nuclear coordinates that are used to define the PES in a nonrelativistic calculation, such as those presented in this paper. For a relativistic calculation, $\hat{H}_{SO} + \hat{V}$ defines the PES, but for the present case we include the spin−orbit operator with the rotational operator as $(\hat{H}_{SO} + \hat{H}_{rot})$ to obtain the rotational structure inclusive of spin−orbit coupling. The spin−orbit Hamiltonian is parametrized by the product $a\zeta_e$,

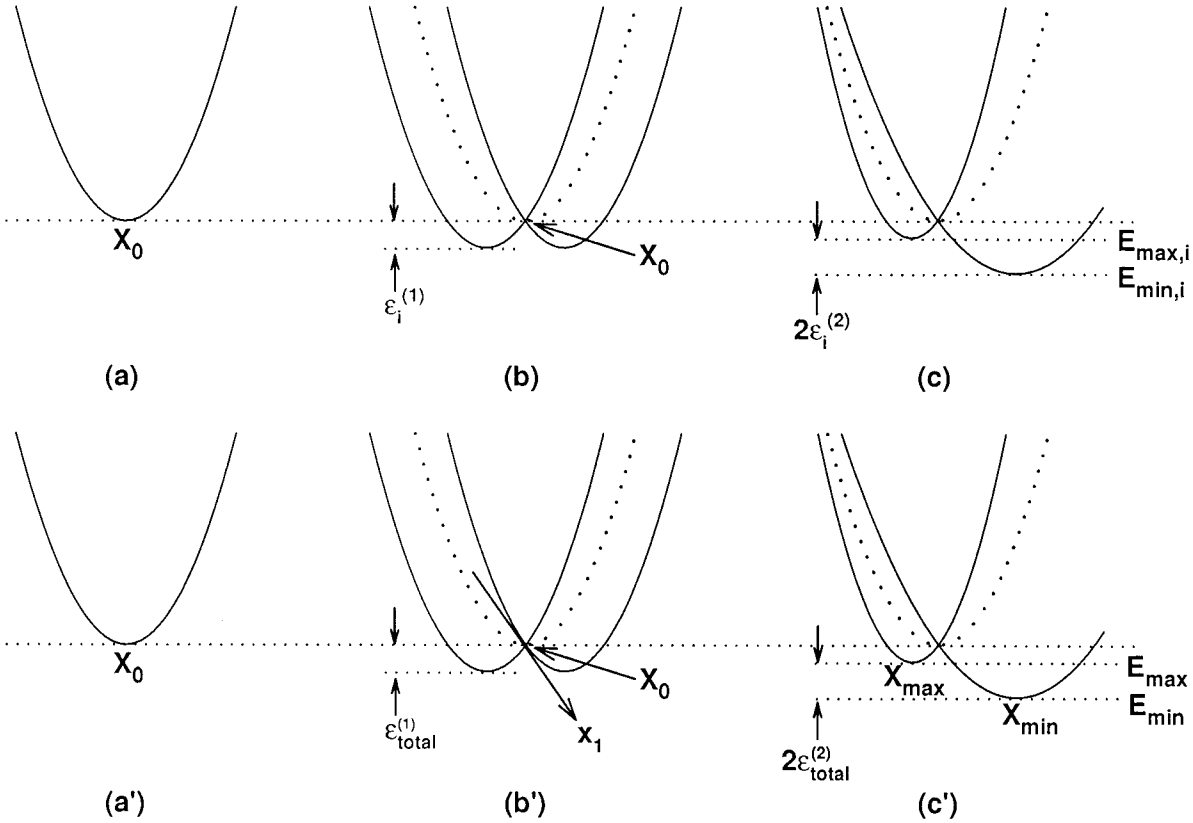

Figure 1. Slices through the Jahn−Teller PES. Curves (a), (b), and (c) are slices through the surface that correspond to $\phi_i = 0$ of the ith Jahn−Teller active mode. Curves (a′), (b′), and (c′) are slices through the surface that contains $\mathbf{X}_0$, $\mathbf{X}_{min}$, and $\mathbf{X}_{max}$. In the limit of a single Jahn−Teller active mode, the slices labeled with and without primes are equivalent; in the general case, they are not. The curves are drawn for the following Hamiltonians: (a) and (a′) harmonic oscillator with zero Jahn−Teller coupling; (b) and (b′) nonzero linear Jahn−Teller coupling; (c) and (c′) nonzero linear and nonzero quadratic Jahn−Teller coupling. In curves (b), (b′), (c), and (c′), the dotted lines are the average potential U_0, which is still a harmonic curve.

where ξ_e is the projection of the electronic orbital angular momentum on the C_3 axis and a is the spin−orbit coupling constant.

The potential energy $\hat{V}$ is conveniently approximated by a Taylor expansion,[19] using the vibrational normal modes as the basis. Each term in the expansion is evaluated at the symmetric configuration, leading to

$$\hat{V} = \hat{H}^0_e + \hat{H}_{h,a_1} + \hat{H}_{h,e} + \hat{H}_1 + \hat{H}_{q_{ii}} + \hat{H}_{q_{ij}} \qquad (2)$$

where the explicit form for each term is given in Table 1.

The parameters of Table 1 are not those that are usually obtained from an analysis of the vibronic structure of a Jahn−Teller active molecule. Instead of the parameter λ_i of $\hat{H}_{h,a_1}$ and $\hat{H}_{h,e}$, the spectral analysis yields the "equilibrium" vibrational frequencies, $\omega_{e,i}$, defined as

$$\omega_{e,i} = \frac{1}{2\pi c}\left(\frac{\lambda_i}{M_i}\right)^{1/2} \qquad (3)$$

where M_i is the reduced mass of the vibrational mode. (The reader should note that the subscript e in $\omega_{e,i}$ does not represent the symmetry of the vibrational mode, but rather stands for "equilibrium." For the Jahn−Teller analyses, the "equilibrium" frequency is taken to be the unperturbed vibrational frequency of the symmetric configuration.)

In addition to being a useful visualization of the state, the PES of the Jahn−Teller state also defines a number of the parameters used in the spectroscopic analyses. For nonzero k_i and g_{ii}, the PES corresponding to a slice through the PES along the ith normal coordinate is given by

$$U_{i,\pm} = \frac{1}{2}\lambda_i\rho_i^2 \pm \rho_i k_i\left[1 + \frac{2g_{ii}\rho_i}{k_i}\cos 3\phi_i + \frac{g_{ii}^2\rho_i^2}{k_i^2}\right]^{1/2} \qquad (4)$$

$$\approx \frac{1}{2}\lambda_i\rho_i^2 \pm (k_i\rho_i + g_{ii}\rho_i^2\cos 3\phi_i) \qquad (5)$$

where in the last equality the expansion of the radical has been truncated at terms quadratic in ρ_i. Figure 1 shows a representation of the PES. (If spin−orbit coupling is included, these equations are modified slightly.[19]) The minima and local maxima of the PES are obtained by finding the roots of eq 5,

$$\rho_{min,i} = \frac{k_i}{\lambda_i(1-K_i)}; \qquad \phi_{min,i} = 0, \frac{2\pi}{3}, \frac{4\pi}{3} \qquad (6)$$

$$E_{min,i} = -\frac{k_i^2}{2\lambda_i(1-K_i)} = -\frac{D_i\omega_{e,i}}{(1-K_i)} \approx -D_i\omega_{e,i}(1+K_i) \qquad (7)$$

$$\rho_{max,i} = \frac{k_i}{\lambda_i(1+K_i)}; \qquad \phi_{max,i} = \frac{\pi}{3}, \pi, \frac{5\pi}{3} \qquad (8)$$

$$E_{max,i} = -\frac{k_i^2}{2\lambda_i(1+K_i)} = -\frac{D_i\omega_{e,i}}{(1+K_i)} \approx -D_i\omega_{e,i}(1-K_i) \qquad (9)$$

These formulas introduce two commonly used Jahn−Teller parameters; D_i is the linear Jahn−Teller coupling constant for the ith mode and K_i is its quadratic Jahn−Teller coupling

constant. Both are dimensionless and are defined in terms of the reduced mass, M_i, of the mode and the parameters of Table 1,

$$D_i = \frac{k_i^2}{2\hbar}\left[\frac{M_i}{\lambda_i^3}\right]^{1/2} \tag{10}$$

and

$$K_i = \frac{g_{ii}}{\lambda_i} \tag{11}$$

These parameters will be used henceforth to describe the Jahn−Teller coupling.

The energies of eqs 7 and 9 are relative to the symmetric configuration, which is defined as the zero of energy. The depth, $\epsilon^{(1)}$, of the moat is the linear Jahn−Teller stabilization energy and is a direct measure of the net effect the Jahn−Teller coupling has on the energy of the molecule. From eqs 7 and 9, the stabilization energy due to linear Jahn−Teller coupling is obtained by setting $K_i = 0$, which yields

$$\epsilon_i^{(1)} = D_i\omega_{e,i} = \frac{k_i^2}{2\lambda_i} \tag{12}$$

The additional stabilization due to quadratic Jahn−Teller coupling in the mode, $\epsilon_i^{(2)}$, is

$$\epsilon_i^{(2)} = D_i\omega_{e,i}K_i \tag{13}$$

The barrier to pseudorotation about the moat is then $2D_i\omega_{e,i}K_i = E_{max,i} - E_{min,i}$.

A common approximation is to assume that the Jahn−Teller stabilization energy of the state is a sum of the Jahn−Teller effect in the individual modes. This approximation results directly from the assumption that the direct cross term $\hat{H}_{q_{ij}}$ of Table 1 is negligible, which all experimental analyses to date have made. It is consistent with the notion that the Jahn−Teller distortion can be accurately represented as the sum of distortions along independent (harmonic) vibrational modes. Under these assumptions, the total Jahn−Teller stabilization energy can be expressed as the sum over each individual mode's contribution,

$$\epsilon_{total} = E_0 - E_{min} \tag{14}$$

$$\approx \sum_{i=1}^{p}(\epsilon_i^{(1)} + \epsilon_i^{(2)}) = \sum_{i=1}^{p} D_i\omega_{e,i}(1 + K_i) \tag{15}$$

This concept is illustrated in Figure 1. The top three curves are labeled with points on the surface and stabilization energies appropriate for a slice through the surface along a given active mode. The bottom three curves are for the slice that corresponds to the "direct" stabilization from $\mathbf{X}_0$ to $\mathbf{X}_{min}$ or $\mathbf{X}_{max}$. We define more rigorously in section 5 the vector $\mathbf{x}_1$, which is the vector of steepest descent from $\mathbf{X}_0$ to $\mathbf{X}_{min}$ or $\mathbf{X}_{max}$, as shown in Figure 1b′,c′.

4. Relationship between the Spectroscopic and *ab Initio* Quantities

One approach to the calculation of the vibronic energy levels of a Jahn−Teller surface would be to exhaustively map the entire PES with an *ab initio* or density functional method. This type of calculation is relatively common for small molecules but still requires arduous calculations of the PES and even more troublesome fitting procedures of the calculated surface to a potential, from which the vibronic and rovibronic quantum levels could be calculated. While in principle this type of approach is possible for a Jahn−Teller active molecule, such calculations have yet to be reported. These calculations will remain prohibitive for quite some time for the larger Jahn−Teller active systems, such as the halogen-substituted benzene cations. As such, a more efficient *ab initio* method is desired.

If the experimental analysis used a Taylor expansion about the minimum of the Jahn−Teller PES, there would be no particular difficulty in the *ab initio* calculation of the expansion parameters of the Taylor expansion. The geometry could be optimized to the minimum and the second, third, and higher derivatives calculated. While not very common, methods to calculate these higher derivatives have been developed for some *ab initio* wavefunctions.[88]

However, as presented in the previous section, the experimental analysis of the Jahn−Teller spin-vibronic structure is most easily accomplished using a Taylor expansion about the symmetric configuration. Because this point is a nonstationary point of the surface, the calculation of the coefficients of the Taylor expansion by *ab initio* methods is not a trivial undertaking. In this section, we describe the relationship between *ab initio* methods and the various quantities that need to be calculated for a complete description of the Jahn−Teller PES of a molecule. We will use as an example of these ideas the ground state of the methoxy family of radicals, which are small enough that high-level *ab initio* calculations can be performed.

4.1. Geometries and Energies. *Calculations at $\mathbf{X}_{min}$ and $\mathbf{X}_{max}$.* By far the most commonly calculated property of Jahn−Teller active molecules is the geometry and total energy of the distorted molecule. These calculations are relatively straightforward to perform, as they require only a single configuration wavefunction and are therefore amenable to the standard programs and methods available via many *ab initio* packages. The distorted molecule can be treated just like any other molecule—the geometry of the distorted configuration can be optimized, and analytical second derivatives, and therefore vibrational frequencies, can be calculated. These calculations are clearly valuable, as they reveal the nature of the distortion, for example, whether distortions in the ground state of methoxy occur along the bond lengths, bond angles, or dihedral angles. Fairly accurate total energies of the global minimum also can be calculated by the use of correlated methods based on single-configuration wavefunctions.

Calculations of the distorted geometries often utilize the symmetry of the electronic state at $\mathbf{X}_{min}$ and $\mathbf{X}_{max}$ of the PES. For example, an E state of a C_{3v} molecule will split into one state each of A′ and A″ symmetry following a distortion that lowers the symmetry of the molecule to C_s. At $\mathbf{X}_{min}$ (in Figure 1c′), the electronic wavefunction transforms as one of these symmetries, while at $\mathbf{X}_{max}$ it transforms as the other. The *ab initio* calculations of these distorted surfaces are perfectly suited to determining the symmetries of the electronic states at these two points.

The calculated total energy and the relative total energies of $\mathbf{X}_{min}$ and $\mathbf{X}_{max}$ are perfectly valid calculations of the value of the energies of the molecule at those points on the PES. If both of these points are located, and confirmed by vibrational frequency calculations, the computed difference in their total energies is an approximation to the stabilization energy due solely to quadratic Jahn−Teller coupling. However, the computed difference will correspond to a sum of the quadratic

TABLE 2: Calculated Geometries and Vibrational Frequencies for X_{min} and X_{max} of the CH_3O Radical[a]

	minimum						maximum			
method	ROHF	UHF	B3LYP	UMP2	CAS	expt[c]	ROHF	UHF	B3LYP	UMP2
energy[b]	−114.416236	−114.420749	−115.050462	−114.420343	−114.686083		−114.416122	−114.420621	−115.050205	−114.685832
r(C−O)	1.384	1.383	1.369	1.388	1.421	1.37	1.385	1.383	1.370	1.390
r(C−H_i)	1.087	1.088	1.111	1.101	1.085	1.10	1.085	1.085	1.102	1.096
r(C−H_o)	1.085	1.085	1.104	1.096	1.085	1.10	1.086	1.087	1.107	1.098
∠(H_i−C−O)	106.1	106.1	105.2	104.8	105.7	110	112.6	112.7	114.9	113.6
∠(H_o−C−O)	111.5	111.6	113.6	112.3	111.2	110	108.3	108.3	108.8	108.0
∠(H_i−C−H_o)	108.6	108.5	110.9	108.0	109.0	109	109.8	109.9	109.6	110.0
ω_1	2843	2833	2916	2895	2843		2843	2836	2936	2903
ω_2	1416	1482	1550	1503	1398	1359	1402	1394	1377	1377
ω_3	993	1078	762	1082	917	1051	1033	1026	1070	1155
ω_4^+	2911	2909	3024	3006	2915	2835	2909	2906	3032	3004
ω_4^-	2905	2892	2986	2976	2857	2835	2908	2894	2974	2977
ω_5^+	1483	1418	1401	1410	1473	1417	1463	1462	1524	1476
ω_5^-	1424	1409	1401	1393	1241	1417	1462	1458	1461	1464
ω_6^+	1083	986	1127	950	1078	1065	1149	1148	1198	1024
ω_6^-	706	726	980	794	1018	1065	742*i*	763*i*	729*i*	836*i*

[a] See section 6 for the computational details. [b] Total energy in hartrees. [c] From Table 5.

stabilization energies of all of the Jahn−Teller active modes; *i.e.*, it will be approximately equal to $\sum_i \epsilon_i^{(2)}$. To make the best comparison with experiment, or to predict the vibronic structure of a state, this sum needs to be apportioned into its individual contributions from the active modes. A rigorous method for accomplishing this feat has not yet been reported; in section 5, we present an approximate method for calculating the quadratic coupling constants, which are fortunately in most cases rather small.

As an example, we show in Table 2 the geometries and energies for $\mathbf{X}_{min}$ and $\mathbf{X}_{max}$ of the ground state of CH_3O calculated via a number of different computational methods. Because it is a small radical with a relatively simple electronic structure, there is not a great deal of difference between the calculated geometries. The calculated bond angles at the minima are the most sensitive parameter to the distortion, and all of the methods agree that at the minimum energy the H_i−C−O angle, where H_i is the unique H atom in the mirror plane of the C_s geometry, is significantly compressed from its tetrahedral value (109.5°) while at the maximum it is correspondingly expanded. Changes in the H_i−C−H_0 methyl scissors angle or the C−H bond lengths r(C−$H_{i/0}$) appear to be relatively minor.

Calculations at the Symmetric Point. One of the most important properties provided by an *ab initio* calculation is the molecule's stabilization energy derived from the Jahn−Teller distortion, i.e., ϵ_{total}, eq 14. While a single-configuration wavefunction can be used for a calculation of the energy of a point on the distorted portion of the PES, a single-configuration wavefunction is wholly inadequate for the calculation at $\mathbf{X}_0$, as shown in several previous works.[32]

At $\mathbf{X}_0$, the degeneracy of the state imposed by the symmetry of the molecule requires that a two-configuration wavefunction be used in the *ab initio* calculation of its energy. Early attempts at these calculations focused on the application of two-configuration self-consistent field methods (TCSCF), which were able to provide reasonable energies of the state. However, until recently, analytical first and second derivatives of the energy were not available for a generalized Hartree−Fock wavefunction. Extensions of the TCSCF were made possible with the advent of the multiconfiguration self-consistent field (MCSCF) methods, which allow for a "state-averaged" wavefunction to be computed. However, only a few calculations at $\mathbf{X}_0$ have been reported using these methods.

It is possible to force the point group symmetry of the molecule to be that at $\mathbf{X}_0$ and to use a one-configuration wavefunction, of a lower symmetry, to calculate an energy. The geometry can also be optimized within the constraints imposed by the higher symmetry of $\mathbf{X}_0$. In this way, an energy can be calculated for the symmetric configuration that can be used with the one-configuration energies of the distorted configurations to estimate a Jahn−Teller stabilization energy. However, the lowest-energy wavefunction at $\mathbf{X}_0$ will be obtained with a two-configuration reference wavefunction, and the one-configuration wavefunction is thus an upper bound on the energy at $\mathbf{X}_0$. (This is strictly true only for those methods that are variational, such as Hartree−Fock wavefunctions. For the other methods, such as those based on Møller−Plesset theory and density functional theory, the one-configuration methods at $\mathbf{X}_0$ are only approximations to the energy at $\mathbf{X}_0$.)

TABLE 3: Calculated Geometries and Energies for X_0 of the CH_3O Radical Using One-Configuration Methods

	ROHF	UHF	B3LYP	UMP2
energy[a]	−114.414498	−114.418982	−115.048120	−114.684718
r(C−O)	1.41	1.41	1.41	1.41
r(C−H)	1.10	1.10	1.10	1.10
∠(H−C−O)	109.1	109.1	109.0	109.0
∠(H−C−H)	109.8	109.8	109.9	109.9
ϵ_{total}[b]	381	388	514	300
$\epsilon_{total}^{(2)}$[c]	25	28	56	55

[a] Total energy in hartrees. [b] Calculated using the energy at $\mathbf{X}_{min}$, Table 2, in cm^{-1}. [c] Calculated using the energies of $\mathbf{X}_{min}$ and $\mathbf{X}_{max}$, Table 2, in cm^{-1}.

In Table 3, we show the calculated geometries and one-configuration wavefunction energies for CH_3O, constrained to C_{3v} symmetry. Because the one-configuration wavefunction is not an appropriate wavefunction for the degenerate electronic state under C_{3v} symmetry, the geometry optimization does not find a minimum on the surface. The one-configuration wavefunction will only be a minimum on the surface belonging to the lower-symmetry point group. The table also lists the calculated stabilization energy ϵ_{total} using the one-configuration energy given in Table 2 for $\mathbf{X}_{min}$. While these calculations of ϵ_{total} may be a relatively good approximation to the experimental value (458 cm^{-1} for CH_3O in Table 5), this approach avoids the problem of calculating the vibrational frequencies and Jahn−Teller coupling constants needed for a determination of the vibronic structure of the molecule.

4.2. Vibrational Frequencies. *Ab initio* calculations of vibrational frequencies are only valid at stationary points on

the surface, such as $\mathbf{X}_{min}$ and $\mathbf{X}_{max}$. However, the experimental analyses of the Jahn−Teller surface use as their starting point the vibrational frequencies at $\mathbf{X}_0$. Therefore, the one-configuration wavefunction calculations of the vibrational frequencies at $\mathbf{X}_{min}$ and $\mathbf{X}_{max}$ are of limited value to the prediction of Jahn−Teller coupling constants. The vibrational frequencies that are often reported for $\mathbf{X}_{min}$ of a Jahn−Teller molecule serve only to verify that a minimum has been found. These frequencies are *not* those obtained from the analysis of the vibronic structure of a Jahn−Teller state. The reason is that the potential is not harmonic in the vicinity of $\mathbf{X}_0$ and $\mathbf{X}_{min}$, and harmonic spacings of the Jahn−Teller active modes are not observed.

As an example of this often poorly understood feature of the Jahn−Teller surface, we show in Table 2 the vibrational frequencies calculated for the ground state of the methoxy radical, as well as those determined experimentally. The table includes vibrational frequencies calculated for $\mathbf{X}_{min}$ and $\mathbf{X}_{max}$ using a variety of one-configuration wavefunctions (ROHF, UHF, UMP2, B3LYP) and a multiconfiguration CASSCF wavefunction. There are some similarities between the frequencies calculated with one-configuration wavefunctions and those either calculated with the two-configuration wavefunction or observed experimentally. However, it is clear from the comparisons shown in the table that the frequencies from the one-configuration wavefunctions would be of extremely limited value as a preliminary step in the analysis of experimental data for these molecules.

One might naively think that the calculated frequency splitting of the Jahn−Teller active modes at $\mathbf{X}_{min}$ will be the splitting observed experimentally. However, the splitting of the vibrational frequencies calculated by the *ab initio* methods for $\mathbf{X}_{min}$ or $\mathbf{X}_{max}$ bears no close relationship to that observed experimentally. For example, the splitting of the $v_i = 1$ level of a Jahn−Teller active mode depends on the equilibrium vibrational frequency $\omega_{e,i}$ and the Jahn−Teller coupling constants D_i and K_i, and possibly the spin−orbit coupling constant $a\zeta_e$ of the state. (For a molecule with more than one Jahn−Teller active mode, the splitting of the lowest vibrational level depends upon all of the Jahn−Teller constants, not just the coupling constant for the mode of interest.) The correlation of these parameters to the two vibrational frequencies that will be calculated for the Jahn−Teller active mode at $\mathbf{X}_{min}$ is minimal at best. For example, in the methoxy radical, the equilibrium vibrational frequency of ν_6 is 1065 cm^{-1}, while Hartree−Fock calculations at the C_s minimum produce vibrational frequencies of 706 and 1083 cm^{-1}. The $v_6 = 1$ level is experimentally observed[12c] to be split by Jahn−Teller and spin−orbit coupling into four levels at energies of 652, 914, 1194, and 1200 cm^{-1}. The disparity is also significant for ν_5, for which the C_s frequencies calculated at the HF level are 1483 and 1424 cm^{-1}, while the experimentally observed energies of $v_5 = 1$ are at 1313, 1403, 1487, and 1492 cm^{-1}. The vibrational frequencies calculated for the C_s geometry cannot easily be corrected to yield the observed vibronic energy levels.

Furthermore, the frequencies of the modes that are not Jahn−Teller active are also not calculated correctly at the distorted configuration. For the modes that are not Jahn−Teller active (for example, the a_1 modes of a C_{3v} molecule), these corrections are so small that no analyses of experimental spectra have yet required them. The relevance to the calculation of vibrational frequencies at $\mathbf{X}_{min}$ is that at the distorted geometry the lower symmetry allows the modes to mix with each other, while they are strictly forbidden from mixing at $\mathbf{X}_0$. For example, upon the lowering of the symmetry of methoxy from C_{3v} to C_s, the *e* modes split into one mode each of a' and a'' symmetry, while the a_1 modes are of a' symmetry. Therefore, the calculation of the a' vibrational frequencies and normal modes at $\mathbf{X}_{min}$ will correspond to admixtures, however slight, of the a_1 and *e* modes of the C_{3v} geometry. The best comparison with the experimentally observed frequencies for a dynamic Jahn−Teller effect will be with frequencies and normal modes calculated for $\mathbf{X}_0$, not for $\mathbf{X}_{min}$. If the Jahn−Teller coupling is so large as to permanently distort the molecule from $\mathbf{X}_0$, the calculations of $\mathbf{X}_{min}$ would be the most appropriate calculations to compare with experiment.

4.3. *Ab Initio* Calculations of the Spin−Orbit Coupling Constants. As we mentioned in the Introduction, almost all Jahn−Teller active molecules have nonzero spin states. In such states, a significant first-order spin−orbit coupling is expected, especially for molecules containing the heavier elements. Therefore, quantum chemical methods that can predict the spin−orbit coupling in these states would also be of value. Spin−orbit coupling is a direct result of relativity, and relativistic methods are required to properly describe it. A great deal of progress has been made in this area over the past decade,[92−95] using both density functional theory and traditional *ab initio* methods. Several types of methods have been used for the calculation of the spin−orbit coupling constants in degenerate states, although all of the methods obtain at best semiquantitative agreement with experiment.[91,92,96,97] We have initiated efforts in using relativistic density functional theory to calculate these constants, with reasonable success.[89,90] However, for the present, we shall confine ourselves to nonrelativistic calculations and treat spin−orbit coupling empirically.

5. Overview of the Computational Approach

The ideal approach is to make no assumptions about the normal modes and vibrational frequencies. However, as previously noted, this requires a frequency calculation at $\mathbf{X}_0$, which is a nonstationary point on the surface. As we present in the next section, we have used *ab initio* methods that calculate the *average* of the two Jahn−Teller surfaces, and in so doing obtain the vibrational frequencies and normal coordinates of all of the vibrational modes of a Jahn−Teller active molecule at the point $\mathbf{X}_0$.

The total energies of the points $\mathbf{X}_0$, $\mathbf{X}_{min}$, and $\mathbf{X}_{max}$ on the surface also are required for a complete description of the Jahn−Teller coupling. A significant advance has been made recently by Robb and co-workers in the implementation of a CASSCF algorithm that is able to optimize the geometry of a molecule at a curve crossing, accidental or otherwise, between two states.[79−82,98] These calculations have proven very successful in the qualitative, and sometimes quantitative, calculation of the photochemistry of organic molecules.[80,99] This method is clearly of interest to the calculation of the Jahn−Teller PES, as it will properly calculate the symmetric configuration of the nuclei as a conical intersection. These calculations provide a truly meaningful total energy of the conical intersection. The conical intersection also determines the vector along which the molecule will distort to remove the degeneracy. Furthermore, if the same active space of orbitals and electrons is used to calculate the energy of the distorted minima and maxima, the total Jahn−Teller stabilization energy can be calculated. These calculations, when coupled with the calculations of the vibrational frequencies of the state, form the basis of our method for the *ab initio* calculation of Jahn−Teller coupling constants.

5.1. Goals. To achieve our goals, the *ab initio* calculations should directly predict the following properties of the state:

- the geometry and total energy, E_0, at the symmetric point, $\mathbf{X}_0$
- the geometries at the minimum, $\mathbf{X}_{\min}$, and at the local maximum, $\mathbf{X}_{\max}$, around the moat (see Figure 1)
- the corresponding total energies $E_{\min}$ and $E_{\max}$ at $\mathbf{X}_{\min}$ and $\mathbf{X}_{\max}$, respectively
- the harmonic frequencies, $\omega_{e,i}$, and normal modes of all of the vibrations, both Jahn−Teller active and inactive
- the linear Jahn−Teller coupling constant D_i and stabilization energy $\epsilon_i^{(1)}$ for each Jahn−Teller active mode
- the quadratic Jahn−Teller coupling constant K_i and stabilization energy $\epsilon_i^{(2)}$ for each Jahn−Teller active mode

The first three items of this list pertain to the nature of the Jahn−Teller distortion and are fundamental to understanding it. The final three parameters are defined by the Jahn−Teller distorted PES and are essential for the calculation of the vibronic energy levels and hence the observed spectra.

The geometries at the conical intersection ($\mathbf{X}_0$), minima ($\mathbf{X}_{\min}$), and maxima ($\mathbf{X}_{\max}$) of the PES are clearly of interest. The total energies at these points are also critical to understanding the distortion of the molecule. The difference in energy between the points $\mathbf{X}_0$ and $\mathbf{X}_{\min}$ is the definition of the total Jahn−Teller stabilization energy, eq 14. The difference between $E_{\min}$ and $E_{\max}$ determines the extent of quadratic Jahn−Teller coupling, eqs 7 and 9. These calculated energies will be used in the calculation of the Jahn−Teller coupling constants.

The vibrational frequencies of the normal modes are defined as being evaluated at $\mathbf{X}_0$. This definition may seem at odds with the requirement that frequencies be calculated at a stationary point on the PES, although as we shall demonstrate, this difficulty can be circumvented. However, the vibrational frequencies and normal modes of $\mathbf{X}_0$ are used as the basis for the Taylor expansion of the potential. The uniqueness of the Jahn−Teller active state is that the first derivatives of the energy with respect to the Jahn−Teller active modes are nonzero and that these derivatives, along with the vibrational frequency, define the linear Jahn−Teller coupling constants, which together with the quadratic coupling constants are critical to understanding the spectra of Jahn−Teller active molecules.

While numerous calculations to date have concentrated on the calculation of the geometry and stabilization energy of the state, very few have attempted to calculate the degenerate vibrational frequencies and Jahn−Teller coupling constants. Our method of calculating these is probably the most novel feature of this work and is also the most useful calculation in aiding the interpretation of the vibronic structure of the state. The closely related stabilization energies $\epsilon_i^{(1)}$ and $\epsilon_i^{(2)}$ for each mode complete our list of objectives for the calculations.

Also of interest to spectroscopists are the rotational constants of the molecule. As with the vibronic structure, the rotational structure of a Jahn−Teller active state is normally approached by adding correction terms to the Hamiltonian appropriate for a symmetric top. For this reason, the symmetric top rotational constants (A_0, B_0, and C_0) determined in a spectral analysis will correspond to the rotational constants at $\mathbf{X}_0$. At sufficiently high resolution, the correction terms h_1^{JT} and h_2^{JT} to the typical symmetric top Hamiltonian can be determined, which will yield the rotational constants at $\mathbf{X}_{\min}$ and $\mathbf{X}_{\max}$.[14−16,100,101]

Our approach to the calculation of a Jahn−Teller PES is quite different from previous attempts. We are able to predict all of the parameters from our list of goals by combining several different types of calculations in the following way. Briefly, our calculations of the Jahn−Teller coupling constants are performed according to the following recipe:

1. The vibrational frequencies and normal modes at $\mathbf{X}_0$ are calculated by generalized restricted Hartree−Fock (GRHF) calculations.
2. The geometry and energy at $\mathbf{X}_0$ are calculated using the CASSCF conical intersection methodology.
3. The geometries and energies at $\mathbf{X}_{\min}$ and $\mathbf{X}_{\max}$ are determined via CASSCF calculations. These energies, along with the conical intersection energy at $\mathbf{X}_0$, give the total linear and quadratic Jahn−Teller stabilization energies.
4. The linear Jahn−Teller coupling constants are calculated by projecting the distortion vector $\mathbf{x}_d$, determined by the CASSCF conical intersection calculation, onto the GRHF normal modes.
5. The quadratic Jahn−Teller coupling constants are calculated by projecting the normal mode corresponding to the imaginary frequency at $\mathbf{X}_{\max}$, calculated at either the CASSCF or ROHF level, onto the GRHF normal modes.

5.2. GRHF Calculations of the "Equilibrium" Vibrational Frequencies. The experimental parameters $\omega_{e,i}$ that are used in the analysis of the vibronic structure of a Jahn−Teller active molecule are defined as the vibrational frequencies of $\mathbf{X}_0$. While $\mathbf{X}_0$ is not a stationary point on the PES, the key to the calculation of the vibrational frequencies is to recognize that the average of the two distorted potentials is a harmonic surface with a minimum at $\mathbf{X}_0$, and its vibrational frequencies correspond to those used in the vibronic analysis. We denote this average potential as U_0, which, for the ith vibrational mode, has the form (eq 5)

$$U_{i,0} = \frac{1}{2}(U_+ + U_-) = \frac{1}{2}\lambda_i \rho_i^2 \tag{16}$$

Clearly, if this average potential U_0 can be calculated, the vibrational frequencies and normal modes can also be calculated.

For a Hartree−Fock wavefunction, the ^{2}E wavefunction arising from an $(e)^3$ configuration is written as a normalized combination of the two components of the e pair of orbitals,

$$^2\mathrm{E(HF)} = \frac{1}{\sqrt{2}}(e_x^2 e_y^1 + e_x^1 e_y^2) \tag{17}$$

In practice, the wavefunction of eq 17 is obtained *via* a generalized restricted Hartree−Fock (GRHF) algorithm available with the CADPAC suite of programs.[102] This package includes analytical second derivatives for a GRHF wavefunction, which makes possible the easy calculation of the vibrational frequencies for the average potential at $\mathbf{X}_0$. One could also calculate this wavefunction using an equally weighted state-averaged CASSCF method, which might seem appropriate since we use the CASSCF method for the calculation of the energies. However, software to calculate vibrational frequencies for such a wavefunction is not yet available. We will therefore use the GRHF wavefunction, which should be sufficiently accurate for our purposes.

Our example is the degenerate wavefunctions of a ^{2}E state, which is appropriate for our benchmark molecules, the methoxy family of radicals. However, the principles of these frequency calculations can be applied to any orbitally degenerate state, including $^2\Pi$ and $^2\Delta$ states of linear molecules and triply degenerate states of molecules that belong to a cubic point group. One advantage of these calculations is the well-known scaling factor for Hartree−Fock vibrational frequencies[57] that can be applied to the GRHF results.

5.3. CASSCF Calculations of the Geometries and Energies of the Critical Points of the PES. As we discussed earlier, the wavefunction for the distorted points on the surface can be calculated using either single-configuration or multiconfiguration methods. As discussed above, we calculate the vibrational frequencies at $\mathbf{X}_0$ with a two-configuration Hartree−Fock wavefunction and single-configuration Hartree−Fock wavefunctions for $\mathbf{X}_{min}$ and $\mathbf{X}_{max}$ are simple to calculate. However, the difference in energy between the two-configuration wavefunction at $\mathbf{X}_0$ and the single-configuration wavefunction at $\mathbf{X}_{min}$ is not a valid calculation of the total Jahn−Teller stabilization energy. The two calculations differ in the number of configurations used and are therefore calculations at two different levels of theory. Thus, the difference in their energies depends upon the computational methods and is nearly meaningless. However, the one-configuration wavefunctions at $\mathbf{X}_{min}$ and $\mathbf{X}_{max}$ are of equal quality, and the difference in energy between their energies should be a good calculation of the total quadratic Jahn−Teller stabilization energy.

We have therefore chosen the CASSCF method for the calculation of the total Jahn−Teller stabilization energy, *i.e.*, the difference $E_0 - E_{min}$. The energy E_0 is calculated as a conical intersection using the CASSCF methodology included in the Gaussian94 quantum chemistry package.[103] The distorted minimum of the PES is then optimized at the CASSCF level using the same active space of electrons and orbitals. This calculation yields the geometry ($\mathbf{X}_{min}$), total energy (E_{min}), and vibrational frequencies of the distorted minimum. As discussed in the previous section, these are not the frequencies used in the prediction of the vibronic structure of the state but are calculated only to verify that a true minimum has been found. The local maximum of the well of the PES can also be optimized, since its electronic state is of different symmetry, yielding its geometry ($\mathbf{X}_{max}$) and energy (E_{max}). Again, the frequencies at the maximum are not particularly useful for understanding the vibronic structure of the state, though we will use the normal mode of the imaginary frequency to predict the quadratic coupling constant.

From the CASSCF calculations we obtain several quantities that can be compared directly with experiment. The rotational constants for $\mathbf{X}_0$ are those determined in a rotationally resolved experiment.[19] The corrections to the rotational constants due to the distorted surface are typically described using the parameters h_1 and h_2, which are related to the rotational constants at $\mathbf{X}_{min}$ and $\mathbf{X}_{max}$.[101] Therefore, the rotational constants calculated for $\mathbf{X}_{min}$ and $\mathbf{X}_{max}$ can be compared with those determined experimentally from the rotational correction terms. Unfortunately, these corrections are generally quite small and have been determined experimentally for only a few molecules, making adequate comparisons of our method with experiment in this area difficult. We will show just one comparison between experiment and theory for CH_3O, though we will provide predictions for the other methoxy radicals.

The linear Jahn−Teller stabilization energy ϵ_{total}, eq 14, is calculated by the CASSCF calculations as the difference in energies of the conical intersection geometry and the minimum geometry, $\epsilon_{total} = E_0 - E_{min}$. The quadratic stabilization energy can also be determined from the CASSCF calculations if $\mathbf{X}_{max}$ is also located. In addition to their intrinsic importance, the calculated stabilization energies form one of the crucial components of our calculation of the Jahn−Teller coupling constants.

5.4. Calculation of the Linear Jahn−Teller Coupling Constants. A conical intersection actually occurs not at a single configuration of the nuclei, but along a "seam" of intersection.[70,81] For a molecule with M vibrational degrees of freedom, the two states will be degenerate along a seam of intersection that corresponds to $M - 2$ degrees of freedom of the molecule. (It is possible that the seam of intersection will occupy $M - 1$ degrees of freedom, but this case is not relevant to the Jahn−Teller problem.) In other words, if the geometry of the molecule is distorted along any one of these $M - 2$ degrees of freedom, the degeneracy of the two surfaces is maintained. In most cases, and the Jahn−Teller surface is one, a minimum of the energy with respect to these $M - 2$ degrees of freedom will exist. The *ab initio* codes that have been developed incorporate gradient methods to find these minima in the intersection space. We use the algorithms developed by Robb and co-workers,[79,81] though we point out that a complementary method has been extensively developed by Yarkony.[74,75,104]

The two degrees of freedom that are not included in the seam of intersection correspond to motions on the PES that lift the degeneracy. Two vectors can be usefully defined,[79,81] the "gradient difference vector" $\mathbf{x_1}$ and the "nonadiabatic coupling" vector $\mathbf{x_2}$. These two vectors span what has been termed[70] the "branching space" of the conical intersection. A distortion of the molecule in the branching space will lift the degeneracy of the conical intersection. For the case of two surfaces "accidentally" crossing, distortion of the molecule from the conical intersection along one of these vectors will lead to the "products" while motion along the other vector will lead to "reactants."

The two vectors $\mathbf{x_1}$ and $\mathbf{x_2}$ are defined as

$$\mathbf{x_1} = \frac{\partial(E_1 - E_2)}{\partial \mathbf{q}} \tag{18}$$

and

$$\mathbf{x_2} = \left\langle E_1 \left| \frac{\partial \hat{H}}{\partial \mathbf{q}} \right| E_2 \right\rangle \tag{19}$$

where $\partial\mathbf{q}$ is an infinitesimal displacement of the Cartesian coordinates of the nuclei[79,81,82] and E_1 and E_2 are the energies of the two wavefunctions that at $\mathbf{X}_0$ are degenerate. For the Jahn−Teller surface, the two vectors $\mathbf{x_1}$ and $\mathbf{x_2}$ are perpendicular to each other. In addition to locating the geometry of the minimum of the seam of intersection and its energy, the CASSCF conical intersection calculation also determines these two vectors. These vectors can be thought of as the steepest descent path from the conical intersection at right angles to one another. In the picture of Figure 1b′, following $\mathbf{x_1}$ on the lower surface will lead to the minimum at $\phi = 0$ while following $\mathbf{x_2}$ corresponds to the slice through $\phi = \pi/2$.

The vector $\mathbf{x_2}$ bears a striking resemblence to the expansion coefficient of the linear term in the Taylor expansion, Table 1. Because $\hat{H}$ of eq 19 is equivalent to $\hat{V}$ of the potential, eq 2, the vector $\mathbf{x_2}$ is the gradient of the electronic state with respect to the $3N$ Cartesian coordinates of the molecule, while k_i is the gradient of the potential with respect to the ith normal mode of the molecule. The relationship between these parameters is given by application of the transformation matrix, $\mathbf{L}$, from normal coordinates, Q_i ($i = 1, ..., 3N - 6$), to Cartesian coordinates, q_α ($\alpha = x_1, y_1, z_1, x_2, ..., z_N$), which we know from the GRHF vibrational calculation,

$$q_\alpha = \sum_{i=1}^{3N-6} l_{\alpha i} Q_i \tag{20}$$

The gradient of the state with respect to the normal modes can then be converted to a sum over the components of the gradient

with respect to Cartesian coordinates,

$$\frac{\partial \hat{V}}{\partial Q_i} = \sum_\alpha \left(\frac{\partial \hat{V}}{\partial q_\alpha}\right)\left(\frac{\partial q_\alpha}{\partial Q_i}\right) = \sum_\alpha l_{\alpha i}\left(\frac{\partial \hat{V}}{\partial q_\alpha}\right) \tag{21}$$

From the definition of k_i (Table 1) and eq 21, we derive the following equation for k_i,

$$\begin{aligned} k_i &= \sum_\alpha l_{\alpha i}\left\langle E_\pm \left| \left(\frac{\partial \hat{V}}{\partial q_\alpha}\right)_0 \right| E_\mp \right\rangle \\ &= \sum_\alpha l_{\alpha i} x_{2\alpha} \\ &= K\sum_\alpha l_{\alpha i} x_{d\alpha} \\ &= K(\mathbf{Q_i}\cdot\mathbf{x_d}) \end{aligned} \tag{22}$$

where K is the magnitude of the vector $\mathbf{x_2}$, $\mathbf{x_d}$ is the unit vector in the direction of $\mathbf{x_2}$, and $x_{2\alpha}$ and $x_{d\alpha}$ are the α components of the vectors $\mathbf{x_2}$ and $\mathbf{x_d}$, respectively. The dot product $\mathbf{Q_i}\cdot\mathbf{x_d}$ is easily obtained from the normal modes of the GRHF calculation and the vector $\mathbf{x_d}$, which is given as part of the Gaussian94 output for a conical intersection calculation. The value of K is not directly obtainable from the output but is easily calculated in the following way.

From the CASSCF conical intersection calculation we know E_0 and from the CASSCF calculation of the minimum of the PES we know E_{min}, and therefore we know the difference between these two energies, ϵ_{total}. If quadratic coupling is small, then the total Jahn−Teller stabilization energy has contributions only from the linear term,

$$\epsilon_{total} = E_0 - E_{min} \approx \sum_{i=1}^{p} \epsilon_i^{(1)} \tag{23}$$

From eq 12, we can rewrite ϵ_{total} as

$$\epsilon_{total} = \sum_{i=1}^{3N-6} \frac{k_i^2}{2\lambda_i} = \sum_{i=1}^{3N-6} \frac{K^2 c_i^2}{2\lambda_i} = K^2 \sum_{i=1}^{3N-6} \frac{c_i^2}{2\lambda_i} \tag{24}$$

where $c_i = \mathbf{Q_i}\cdot\mathbf{x_d}$. The summations are shown as being taken over all $3N - 6$ normal modes, but only the Jahn−Teller active modes will have nonzero c_i. All of the variables of eq 24 are known from either the CASSCF calculations (ϵ_{total} and $\mathbf{x_d}$) or the GRHF calculations ($\mathbf{Q_i}$ and λ_i) with the exception of K, whose value can then be calculated as

$$K^2 = \epsilon_{total}\left(\sum_{i=1}^{3N-6} \frac{c_i^2}{2\lambda_i}\right)^{-1} \tag{25}$$

The individual Jahn−Teller stabilization energies can then be calculated as

$$\epsilon_i^{(1)} = \frac{k_i^2}{2\lambda_i} = \frac{c_i^2 K^2}{2\lambda_i} = \frac{c_i^2 \epsilon_{total}}{2\lambda_i \sum_{i'=1}^{3N-6} \frac{c_{i'}^2}{2\lambda_{i'}}} \tag{26}$$

Coupling eq 26 with eq 12 yields an equation for the linear Jahn−Teller coupling constant,

$$D_i = \frac{\epsilon_i^{(1)}}{\omega_{e,i}} \tag{27}$$

for which the value of $\omega_{e,i}$ has been determined by the GRHF calculation.

Any error in the *ab initio* calculations of $\epsilon_{total} = E_0 - E_{min}$ will be propagated into the calculation of $\epsilon_i^{(1)}$ and D_i. For example, if the quantity $E_0 - E_{min}$ is calculated in error by the CASSCF calculations by some factor, then all of the linear coupling constants and stabilization energies will be in error by that same factor. However, their relative sizes will not be affected by this error. On the other hand, if the distortion vector $\mathbf{x_d}$ is not accurately predicted by the conical intersection calculation, then the relative contributions of the D_i and $\epsilon_i^{(1)}$ will be affected. The same conclusion applies if the frequencies or the normal modes are calculated incorrectly.

5.5. Calculation of the Quadratic Jahn−Teller Coupling Constants. If the second derivatives of the energy with respect to the Cartesian coordinates were also calculated at the conical intersection, the quadratic coupling constants for each active mode could be determined in an analogous fashion to the calculation of the linear coupling constants. However, the implementation in the current *ab initio* programs include only the first derivatives of the energy. We have therefore adopted a less rigorous, but still qualitatively correct, approach for the calculation of the typically much smaller quadratic Jahn−Teller stabilization energies for each vibrational mode.

As we discussed earlier, a single-configuration wavefunction is acceptable for the calculation of the geometry and energy of the lower symmetry sections of the PES. In particular, a calculation at $\mathbf{X}_{max}$ is the location of a transition state to the pseudorotation of the molecule about the moat in the PES. While the second derivatives at $\mathbf{X}_{max}$ are not equivalent to those at $\mathbf{X}_0$, the normal mode of the imaginary frequency of the transition state calculation at $\mathbf{X}_{max}$ should closely correspond to the mode or modes that have quadratic Jahn−Teller activity. We therefore approximate the individual mode's quadratic Jahn−Teller stabilization energy in the following way.

The normal mode, $\mathbf{x}_{max}$, for the imaginary frequency of the transition state calculation at $\mathbf{X}_{max}$ is the motion of steepest descent from $\mathbf{X}_{max}$ to $\mathbf{X}_{min}$. If only one vibrational mode of the molecule were Jahn−Teller active, $\mathbf{x}_{max}$ would be exactly ϕ (Figure 1c′). For the general case, we apportion the contributions of the different vibrational modes to $\mathbf{x}_{max}$ by projecting $\mathbf{x}_{max}$ onto the normal modes from the GRHF calculation,

$$\mathbf{x}_{max} \approx \sum_i c_i' Q_{i,\pm} \tag{28}$$

We then combine eq 28 with the *ab initio* calculations of the quadratic Jahn−Teller stabilization energy $\epsilon_{total}^{(2)} = {}^1/_2(E_{max} - E_{min})$ and its definition in terms of the quadratic coupling constants, eq 13, to obtain

$$\epsilon_i^{(2)} = \frac{1}{2}(c_i')^2(E_{max} - E_{min}) \tag{29}$$

$$K_i = \frac{\epsilon_i^{(2)}}{D_i \omega_{e,i}} \tag{30}$$

In all of the radicals and ions studied in this paper, the quadratic stabilization is extremely small compared to the linear

stabilization energy, which is already on the order of only a few hundred cm^{-1}. The challenge is therefore finding a computational method that finds both a maximum and a minimum on the PES and also provides a reasonably accurate calculation of the difference in energy between them. As we discussed in the previous section, $\mathbf{X}_{min}$ and $\mathbf{X}_{max}$ usually correspond to different symmetries of the electronic wavefunction. Furthermore, single-configuration methods are appropriate for the calculation of the wavefunctions for $\mathbf{X}_{min}$ and $\mathbf{X}_{max}$, which means that single-configuration HF calculations or the multiconfiguration CASSCF methods can be used.

We have actually had the most success in these calculations using the restricted open-shell Hartree−Fock method rather than the CASSCF wavefunctions. For the methoxy family of radicals, the ROHF calculations do predict minima and maxima on the surface, albeit the calculated differences in energy vary from only 9 cm^{-1} in the case of CH_3S to the largest of 25 cm^{-1} in CH_3O. These results will be discussed for each radical.

6. Computational Details

6.1. CASSCF Calculations. The CASSCF calculations of $\mathbf{X}_0$, $\mathbf{X}_{min}$, and $\mathbf{X}_{max}$ were performed using Gaussian94.[103] Two critical choices had to be made concerning the size of the active space and the basis set. Unfortunately, the CASSCF calculations are quite time-intensive and limitations had to be placed on each of these choices. The results quoted in the remainder of the paper were obtained using an active space of 5 electrons and 6 orbitals with a 6-31G* basis set. The valence electronic structure of the CX_3Y radicals can be summarized as [C−X σ bonds][X lone pairs]$(1a_1)^2(2a_1)^2(1e)^3(3a_1)^0$[virtuals]. The $1a_1$ orbital is nominally the Y $ns\sigma$ lone pair, the $2a_1$ orbital is the C−Y σ bond, the $1e$ orbital is the Y $np\pi$ lone pairs, and the $3a_1$ orbital is the C−Y σ^* orbital. The $2a_1$, $1e$, $3a_1$, and a virtual orbital that approximated the $(n + 1)p\pi$ orbital of Y were the active space. For CH_3O only, we investigated smaller and larger active spaces as well as a 6-31G** basis set. The predictions of the Jahn−Teller coupling constants were not significantly affected by the change in active space or basis set.

In practice, $\mathbf{X}_{min}$ was found by starting the geometry optimization near the geometry $\mathbf{X}_0$, located by the conical intersection calculation. The standard optimization algorithms would usually then locate $\mathbf{X}_{min}$ automatically. To find $\mathbf{X}_{max}$, the initial geometry used was that of $\mathbf{X}_{min}$, but the symmetry of the electronic state was swapped. For example, if the minimum corresponded to a state of $^2A'$ symmetry under the C_s point group, then the maximum was usually located as the $^2A''$ state. In each case, the location of a minimum or maximum was verified by a vibrational frequency calculation. No local minima in the PES could be found at the CAS level for any of the CX_3Y radicals. For this reason, the ROHF calculations of the maximum and minimum energies were used in the calculation of the quadratic stabilization energies.

6.2. GRHF Calculations. The GRHF calculations were performed using the CADPAC package of programs[102] with a 6-31G* basis set. The Coulomb and exchange coupling coefficients were entered as described in the manual[105] for a $(\pi)^3$ configuration of a linear molecule. As with the CASSCF calculations, a test calculation on CH_3O using a larger basis set (6-31G**) had a negligible effect on the calculation of the vibrational frequencies and normal modes, and hence the Jahn−Teller coupling constants. The ROHF calculations of the minima and maxima were also performed with the CADPAC software.

6.3. Calculations of the Distorted Geometry. The calculations reported in Table 2 were all done using a 6-31G* basis set. The restricted open-shell Hartree−Fock (ROHF) calculations were performed with the CADPAC program, which has analytical second derivatives available. The unrestricted Hartree−Fock (UHF), unrestricted Møller−Plesset (UMP2), and hybrid Hartree−Fock/density functional B3LYP calculations were all done with the Gaussian94 program. The CASSCF active space was identical to that used in the calculation of the Jahn−Teller stabilization energy.

6.4. Projection of $\mathbf{x_d}$ onto the GRHF Normal Modes. A short computer program was written to perform the projection of the vector $\mathbf{x_d}$ onto the normal modes from the GRHF calculation. The major task of this program is to extract the relevant information from the output files and to remove the mass weighting from the vibrational normal modes for the calculation of the linear and quadratic coupling constants. The program is available upon request from one of the authors.

7. Results and Discussion for the Methoxy Family of Radicals

7.1. CH_3O. The methoxy radical has been intensely scrutinized by electronic structure calculations. Three topics have been investigated the most—the nature of the Jahn−Teller distortion in the ground state,[51,52] the isomerization along the ground-state surface to CH_2OH,[106] and its excited states.[107]

All of the calculations of the ground state distortion agree that the minimum and maximum of the PES correspond to $^2A'$ and $^2A''$ symmetries of the electronic wavefunction, respectively. Our ROHF and CASSCF calculations of these points on the PES are listed in Table 4, and a further collection of calculations can be found in the review by Cook.[52] It is significant that the largest changes in the geometry are in the bond angles. It is therefore expected that the vibrational modes that involve the bond angles the most should show the greatest Jahn−Teller activity.

Table 5 contains the experimentally determined Jahn−Teller parameters for all four of the CX_3Y radicals along with the values calculated using our *ab initio* algorithm detailed earlier. These parameters include the six vibrational frequencies (three Jahn−Teller inactive modes (ν_1, ν_2, and ν_3) and three Jahn−Teller active modes (ν_4, ν_5, and ν_6)), the three linear Jahn−Teller coupling constants and corresponding stabilization energies, and the quadratic stabilization energies for each mode. The table also includes the geometry obtained from the CASSCF conical intersection calculation and a comparison of it with the experimentally determined structure obtained from the rotational constants of the symmetric point of the surface.

It is not surprising that the vibrational frequencies should agree reasonably well between the experiments and the Hartree−Fock calculations, given that the latter are scaled by an empirical[57] factor. Both the experimental analysis and the calculations agree that the mode showing the most Jahn−Teller activity is ν_6, which is nominally the methyl rocking motion, or alternatively, the tilting of the O atom off the C_3 axis. The agreement between the calculations and the experimental value of D_6 is extremely good, and in fact is probably better than could have been expected.

The quadratic Jahn−Teller coupling in all of the methoxy radicals is quite small, as both the experiments and *ab initio* calculations have shown. In fact, at the CASSCF level, we were unable to locate maxima about the moat for any of the four radicals. However, at the ROHF level, maxima were located and it is the imaginary normal mode from the ROHF calculation and the difference in energy between the ROHF minimum and ROHF maximum that were used in the calculation of the

TABLE 4: Calculated Geometries and Vibrational Frequencies for the Minima and Maxima of the Ground State of the CX_3Y Radicals[a,b]

	CH_3O			CF_3O			CH_3S			CF_3S		
	min		max	min		max	min		max	min		max
symmetry	ROHF $^2A'$	CAS $^2A'$	ROHF $^2A'$	ROHF $^2A'$	CAS $^2A'$	ROHF $^2A''$	ROHF $^2A'$	CAS $^2A'$	ROHF $^2A''$	ROHF $^2A'$	CAS $^2A'$	ROHF $^2A''$
r(C−Y)	1.384	1.421	1.385	1.353	1.384	1.353	1.809	1.814	1.809	1.803	1.807	1.804
r(C−X_i)	1.087	1.085	1.085	1.306	1.306	1.310	1.085	1.085	1.080	1.316	1.316	1.315
r(C−X_o)	1.085	1.085	1.086	1.308	1.309	1.307	1.081	1.081	1.083	1.315	1.316	1.315
∠(Y−C−X_i)	106.1	105.7	112.6	106.9	106.8	112.3	107.4	107.4	111.8	108.6	112.2	112.9
∠(Y−C−X_o)	111.5	111.2	108.3	111.3	111.3	108.5	111.0	111.2	108.8	112.1	108.7	110.0
∠(X_i−C−X_o)	108.6	109.0	109.8	109.7	109.8	108.5	108.5	108.4	109.7	108.3	108.2	107.6
∠(X_o−C−X_o)	110.4	110.5	107.9	107.9	107.9	110.5	110.3	110.1	107.9	107.2	107.1	108.7
$\omega_{e,1}$	2843	2843	2843	1308	1287	1307	2867	2867	2869	1151	1143	1151
$\omega_{e,2}$	1416	1398	1402	881	851	881	1343	1348	1342	749	743	749
$\omega_{e,3}$	993	917	1033	606	595	606	687	673	689	443	438	443
$\omega^+_{e,4}$	2911	2915	2909	1275	1232	1277	2946	2945	2959	1223	1222	1221
$\omega^-_{e,4}$	2905	2857	2908	1274	1228	1272	2937	2935	2912	1217	1219	1216
$\omega^+_{e,5}$	1483	1473	1463	581	593	594	1448	1449	1431	525	534	526
$\omega^-_{e,5}$	1424	1241	1462	571	577	555	1394	1399	1420	525	524	524
$\omega^+_{e,6}$	1083	1078	1149	411	415	403	881	891	960	297	318	315
$\omega^-_{e,6}$	706	1018	742i	212	315	242i	559	648	651i	182	203	196i

[a] Both the ROHF and CAS frequencies have been scaled by 0.89.[57] [b] Bond lengths are in Å, bond angles in degrees, and vibrational frequencies in cm^{-1}.

TABLE 5: Comparison of the Experimental and Calculated Geometries, Vibrational Frequencies, Jahn−Teller Coupling Constants, Jahn−Teller Stabilization Energies, and Spin−Orbit Coupling Constants for the Ground States of the CX_3Y Radicals (Experimental Values from Ref 19)[a]

	CH_3O		CF_3O		CH_3S		CF_3S	
parameter	expt	calc	expt	calc	expt	calc	expt	calc
r(C−O)	1.37	1.426	1.361	1.388	1.767	1.817	1.828	1.810
r(C−X)	1.10	1.085	1.327[b]	1.308	1.10[b]	1.082	1.327[b]	1.316
∠(Y−C−X)	110	109.4	109.6	109.8	115.8	109.9	109.5	111.1
∠(X−C−X)	109	109.6	109.3	109.1	102.5	109.0	109.5	107.8
$\omega_{e,1}$	*c*	2822	1215	1305	2776	2851	1142	1151
$\omega_{e,2}$	1359	1422	977	881	1313	1330	765	749
$\omega_{e,3}$	1051	1040	527	606	717	689	449	442
$\omega_{e,4}$	2835	2891	*c*	1276	*c*	2932	*c*	1220
D_4	0.02	<0.01	*c*	<0.01	*c*	<0.01	*c*	0.0
$\epsilon_4^{(1)}$	57	≈2	*c*	≈0	*c*	≈6	*c*	0
$\epsilon_4^{(2)}$	*c*	2	*c*	4	*c*	12	*c*	0
$\omega_{e,5}$	1417	1434	600	583	*c*	1422	536	525
D_5	0.075	0.02	0.04	0.04	*c*	0.02	0.0	0.0
$\epsilon_5^{(1)}$	106	33	24	23	*c*	22	0	0
$\epsilon_5^{(2)}$	3	3	*c*	3	*c*	4	*c*	0
$\omega_{e,6}$	1065	1082	465[d]	410	913[b]	913	320	309
D_6	0.24	0.20	0.45	0.55	0.045	0.16	0.24	0.70
$\epsilon_6^{(1)}$	256	221	233	226	41	144	77	217
$\epsilon_6^{(2)}$	36	20	12	3	*c*	*2*	*c*	10
ϵ_{total}	458	256	245	249	41	171	77	217
$a\zeta_e$	−140		−145		−340		−360	

[a] Bond lengths are in Å, bond angles are in deg, and the vibrational frequencies, Jahn−Teller stabilization energies, and spin−orbit constants are in cm^{-1}. The linear Jahn−Teller coupling constants are dimensionless. [b] Fixed at the *ab initio* value. [c] This parameter was not determined in the experimental analyses. [d] For CF_3O, an anharmonicity in ν_6 was used in the simulations, $\omega_e x_e = 8$ cm^{-1}.

quadratic Jahn−Teller stabilization energies. In Table 5 we quote not the quadratic Jahn−Teller coupling constants K_i but instead the quadratic Jahn−Teller stabilization energy for each mode, $\epsilon_i^{(2)}$. We have chosen this representation because of the error associated with the calculation of those linear vibrational coupling constants that are quite small (D_4 and D_5 in CH_3O). From eq 30, any error in the prediction of D_i will be carried through as an error in K_i. For ν_5 and ν_4, the percent error in D_i is quite large, but the total error is not. Therefore, we have used

TABLE 6: Calculated Jahn−Teller Corrections to the Symmetric Top Rotational Constants of the CX_3Y Radicals, in cm^{-1}

molecule	$h_1^{(JT)}$	$h_2^{(JT)}$
CH_3O	6×10^{-4}	3.0×10^{-2}
CF_3O	5×10^{-5}	3.9×10^{-3}
CH_3S	3×10^{-5}	1.3×10^{-2}
CF_3S	5×10^{-4}	4.5×10^{-3}

$\epsilon_i^{(2)}$, calculated via eqs 28 and 29, as the point of comparison between experiment and the calculations because it will not contain the error associated with D_i. It can be seen in Table 5 that the agreement between the calculated and experimental values of $\epsilon_i^{(2)}$ is quite good, especially given the small size of these values.

As with the analysis of the vibrational structure of a Jahn−Teller active molecule, the rotational structure is most easily derived by beginning with the rotational constants of the symmetric top at $\mathbf{X}_0$. Corrections, generally quite small, are then made to the symmetric top Hamiltonian to reproduce the observed rotational energy levels of the molecule. Elsewhere[19] we have shown how, based on a theoretical approach originally developed by Watson,[101] the Jahn−Teller coupling constants, vibrational frequencies, and rotational constants can be used to calculate the Jahn−Teller corrections to the symmetric top rotational constants. These calculations involve the use of the centrifugal derivatives of the vibrational modes, which can be readily calculated from the *ab initio* normal modes.[109] We show in Table 6 the calculated rotational correction terms $h_1^{(JT)}$ and $h_2^{(JT)}$ for all four CX_3Y radicals. A comparison of the calculated and experimental values can be made only for CH_3O, for which the experimental values[19] are $h_1^{(JT)} = 3.38(3) \times 10^{-4}$ cm^{-1} and $h_2^{(JT)} = 7.81(2) \times 10^{-2}$ cm^{-1}. Given the small size of these parameters, it is satisfying that the calculations obtain the correct order of magnitude for them.

In Figure 2 we show two simulations of the dispersed fluorescence from the 6^1 level of the excited state of CH_3O. The spin-vibronic energy levels and transition intensities were calculated using a program we have described in detail elsewhere.[19] We have chosen this spectrum as it highlights the majority of the Jahn−Teller active levels. Because of the large

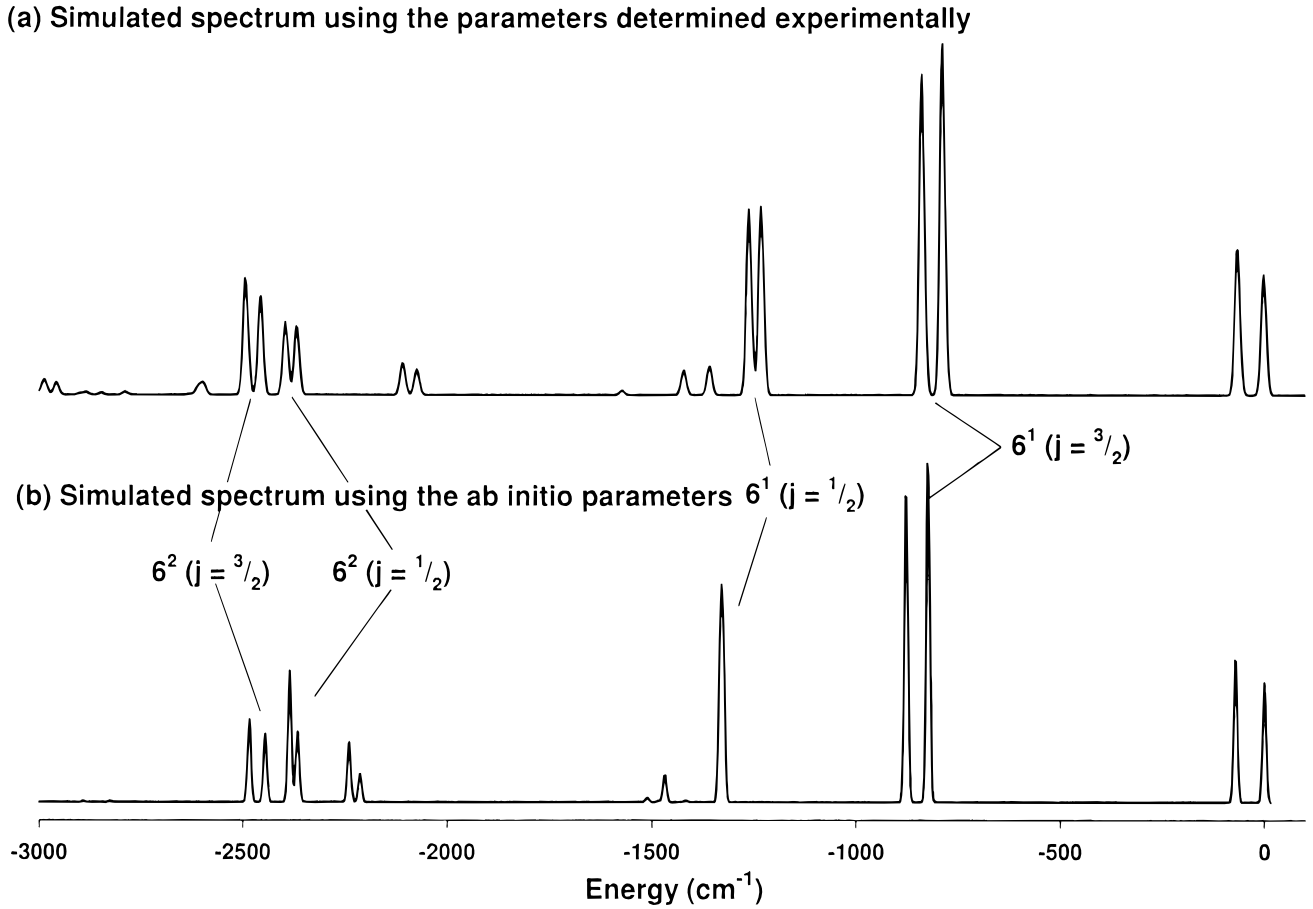

Figure 2. Simulations of the dispersed fluorescence of CH_3O from the 6^1 level. (a) Simulation using the experimentally obtained constants with the quadratic coupling constants set to zero. (b) Simulation using the coupling constants predicted by this work, with the quadratic coupling constants set to zero. Because the *ab initio* calculation does not predict a spin−orbit coupling constant, the value for $a\zeta_e$ was taken to be the same as the experimentally determined value, -140 cm^{-1}. The peak at $\approx$1300 cm^{-1} is actually two transitions only 7 cm^{-1} apart.

error in the prediction of the quadratic coupling constants, we have omitted them from the simulations. This is not a major problem as the effects of quadratic coupling in the spectra are quite evident once the effects of linear coupling have been determined.

Figure 2 shows how close we have come to our goal of predicting the spin-vibronic energy levels and the electronic spectra for a Jahn−Teller active state. The most important feature of the spectrum is the large splitting and shifting of the $\nu_6 = 1$ level, designated 6^1 ($j = 1/2$) and 6^1 ($j = 3/2$). The energies of these levels predicted by the *ab initio* calculations are in reasonable agreement with those found experimentally. Furthermore, the intensities of the electronic transitions to these levels, relative to the origin (0^0 ($j = 1/2$)), are also in good agreement with the experimental intensities. Starting from the *ab initio* simulation, it would be a straightforward process to adjust the constants to obtain the experimentally observed spectrum. The agreement for the levels that are predominantly ν_5 and ν_4, the weaker features at higher energies, is not as good because of the error in the prediction of D_5 and D_4. However, the predicted vibrational frequencies for these modes are quite good and the predicted linear coupling constants are of the correct order of magnitude.

7.2. CF_3O. Several previous *ab initio* calculations have been performed on the ground and excited states of the CF_3O radical, though none of them have reported calculations of the Jahn−Teller coupling constants.[53] Most of these calculations were concerned with the atmospheric fate of CF_3O after its possible production from the oxidation of chlorofluorocarbons in the upper atmosphere. Our calculations in Table 5 represent the first calculations of the vibrational frequencies for the symmetric configuration.

As with the CH_3O radical, the calculations perform quite admirably, correctly predicting that ν_6 is by far the most active mode in the radical. Again, somewhat surprisingly, the calculations are even in good quantitative agreement with respect to the sizes of the linear coupling constant. This is an even more impressive achievement than in CH_3O, given the greater effect the fluorines will have on the electronic structure of the radical.

7.3. CH_3S and CF_3S. The agreement between experiment and theory for CH_3S and CF_3S is qualitatively very good, but is quantitatively not as good as the agreement for CH_3O and CF_3O. From Table 5, it can be seen that the calculations and experiment both agree that ν_6 is the mode with the greatest linear Jahn−Teller coupling, with minor contributions from ν_5 and ν_4. However, they disagree on the magnitude of the interaction, with the calculations overestimating it by a factor of 3 in each radical. This discrepancy can be traced entirely to the calculation of the total Jahn−Teller stabilization by the two CASSCF calculations. If these two calculations overestimate the stabilization energy by some factor, then the linear coupling constants will be overestimated by the same factor. Given the limited basis set and, probably more importantly, the limited size of the active space in the CASSCF calculations, it is not surprising that the stabilization energy should be calculated erroneously. However, it is important to note that the distortion vector from the conical intersection calculation and its decomposition into contributions from the normal modes is still a quite good calculation—both

the experiments and calculations agree that the Jahn−Teller coupling is almost entirely contained in ν_6. We expect that calculations with a larger active space and calculations that include dynamical electron correlation would likely improve the calculation of the Jahn−Teller stabilization energy, and hence the calculation of the magnitude of the linear coupling constants.

8. Conclusions

In this work, we have made the first attempts to quantitatively calculate, via *ab initio* methods, the spectroscopic parameters that characterize the Jahn−Teller potential energy surface. The method that we have developed calculates the vibrational frequencies, as well as the linear and quadratic Jahn−Teller coupling constants for an orbitally degenerate electronic state of nonlinear molecules. The method relies on the use of three different types of calculations—GRHF calculations of the vibrational frequencies and normal modes, a CASSCF calculation of the symmetric configuration as a conical intersection, and CASSCF calculations of the minimum of the PES. When combined, these calculations can predict to at least qualitative, if not quantitative, accuracy the vibronic parameters and structure of the state.

In the Introduction, we argued that our calculations should be of value in the interpretation of the experimental data. While some of the calculations clearly leave room for improvement (such as the prediction of the quadratic Jahn−Teller coupling constants), we feel that indeed we have made clear progress toward this goal with our algorithm for the calculation of the Jahn−Teller parameters.

Our future work in this area will be directed in several areas. First, extension to the prediction of the coupling constants in the aromatic cations and radicals is clearly desirable, as an extensive array of experiments have been performed on them.[23] Second, the effects of dynamic electron correlation should be included in the calculation of the conical intersection calculation. (For example, the inclusion of electron correlation in the *ab initio* method reduced the calculated Jahn−Teller stabilization energy in VCl_4 significantly.[91]) Finally, for a complete prediction of observed spectra, *ab initio* values of the spin−orbit coupling constant are required.

Acknowledgment. We thank the National Science Foundation (T.A.M., Grant No. CHE-9320909) for funding this research. All of the calculations were performed at the Ohio Supercomputing Center (Grant No. PAS540). T.A.B. thanks the The Ohio State University for fellowship support.

References and Notes

(1) Jahn, H. A.; Teller, E. *Proc. R. Soc. A* **1937**, *161*, 220−235.

(2) Chancey, C. C.; O'Brien, M. C. M. *The Jahn−Teller Effect in C_{60} and Other Icosahedral Complexes*; Princeton University Press: Princeton, NJ, 1997.

(3) Huheey, J. E.; Keiter, E. A.; Keiter, R. L. *Inorganic Chemistry: Principles of Structure and Reactivity*, 4th ed.; HarperCollins: New York, 1993.

(4) Kaplan, M. D.; Vekhter, B. G. *Cooperative Phenomena in Jahn−Teller Crystals*; Plenum: New York, 1995.

(5) Falvello, L. R. *J. Chem. Soc., Dalton Trans.* **1997**, *23*, 4463−4476.

(6) Sturge, M. D. *Solid State Phys.* **1967**, *20*, 91−211.

(7) Köppel, H. *Z. Phys. Chem.* **1997**, *200*, 3−10.

(8) Miller, T. A.; Bondybey, V. E. In *Molecular Ions: Spectroscopy, Structure, and Chemistry*. Miller, T. A., Bondybey, V. E., Eds.; North-Holland: Amsterdam, 1983.

(9) Johnson, K. H. *Fusion Technol.* **1994**, *26*, 427−430.

(10) (a) Berry, M. V. *Proc. R. Soc. London, Ser. A* **1984**, *392*, 45−57. (b) Koizumi, H.; Sugano, S. *J. Chem. Phys.* **1994**, *101*, 4903−4913. (c) Schön, J.; Köppel, H. *J. Chem. Phys.* **1995**, *103*, 9292−9303. (d) Schön, J.; Köppel, H. *J. Chem. Phys.* **1998**, *108*, 1503−1513.

(11) Miller, T. A. *Science* **1984**, *223*, 545−553.

(12) (a) Brossard, S. D.; Carrick, P. G.; Chappell, E. L.; Hulegaard, S. C.; Engelking, P. C. *J. Chem. Phys.* **1986**, *84*, 2459−2465. (b) Inoue, G.; Akimoto, H.; Okuda, M. *Chem. Phys. Lett.* **1979**, *63*, 213−216. (c) Geers, A.; Kappert, J.; Temps, F.; Sears, T. J. *J. Chem. Phys.* **1993**, *98*, 4297−4300. (d) Foster, S. C.; Misra, P.; Lin, T.-Y. D.; Damo, C. P.; Carter, C. C.; Miller, T. A. *J. Phys. Chem.* **1988**, *92*, 5914−5921. (e) Lee, Y.-Y.; Wann, G.-H.; Lee, Y.-P. *J. Chem. Phys.* **1993**, *99*, 9465−9471. (f) Liu, X.; Foster, S. C.; Williamson, J. M.; Yu, L.; Miller, T. A. *Mol. Phys.* **1990**, *69*, 357−367. (g) Liu, X.; Yu, L.; Miller, T. A. *J. Mol. Spec.* **1990**, *140*, 112−125. (h) Momose, T.; Endo, Y.; Hirota, E.; Shida, T. *J. Chem. Phys.* **1988**, *88*, 5338−5343. (i) Momose, T.; Endo, Y.; Hirota, E. *J. Chem. Phys.* **1989**, *90*, 4636−4637. (j) Carrick, P. G.; Brossard, S. D.; Engelking, P. C. *J. Chem. Phys.* **1985**, *83*, 1995−1996.

(13) Engelking, P. C.; Ellison, G. B.; Lineberger, W. C. *J. Chem. Phys.* **1978**, *69*, 1826−1832.

(14) Endo, Y.; Saito, S.; Hirota, E. *J. Chem. Phys.* **1984**, *81*, 122−135.

(15) Radford, H. E.; Russell, D. K. *J. Chem. Phys.* **1977**, *66*, 2222−2224.

(16) Russell, D. K.; Radford, H. E. *J. Chem. Phys.* **1980**, *72*, 2750−2759.

(17) (a) Suzuki, M.; Inoue, G.; Akimoto, H. *J. Chem. Phys.* **1984**, *81*, 5405−5412. (b) Chiang, S.-Y.; Lee, Y.-P. *J. Chem. Phys.* **1991**, *95*, 66−72. (c) Endo, Y.; Saito, S.; Hirota, E. *J. Chem. Phys.* **1986**, *85*, 1770−1777.

(18) (a) Li, Z.; Francisco, J. S. *Chem. Phys. Lett.* **1991**, *186*, 336−342. (b) Tan, X.-Q.; Yang, M.-C.; Carter, C. C.; Williamson, J. M.; Miller, T. A.; Mlsna, T. E.; Anderson, J. D. O.; Desmarteau, D. D. *J. Phys. Chem.* **1994**, *98*, 2732−2734.

(19) Barckholtz, T. A.; Miller, T. A. *Int. Rev. Phys. Chem.* **1998**, *17*, 435−529.

(20) Barckholtz, T. A.; Powers, D. E.; Miller, T. A.; Bursten, B. E. *J. Am. Chem. Soc.*, in press.

(21) (a) Engelking, P. C.; Lineberger, W. C. *J. Chem. Phys.* **1977**, *67*, 1412−1417. (b) Yu, L.; Williamson, J. M.; Miller, T. A. *Chem. Phys. Lett.* **1989**, *162*, 431−436. (c) Yu, L.; Foster, S. C.; Williamson, J. M.; Heaven, M. C.; Miller, T. A. *J. Phys. Chem.* **1988**, *92*, 4263−4266. (d) Yu, L.; Cullin, D. W.; Williamson, J. M.; Miller, T. A. *J. Chem. Phys.* **1993**, *98*, 2682−2698.

(22) (a) Long, S. R.; Meek, J. T.; Reilly, J. P. *J. Chem. Phys.* **1983**, *79*, 3206−3219. (b) Lindner, R.; Sekiya, H.; Beyl, B.; Müller-Dethlefs, K. *Angew. Chem., Int. Ed. Engl.* **1993**, *32*, 603−606. (c) Lindner, R.; Müller-Dethlefs, K.; Wedum, E.; Haber, K.; Grant, E. R. *Science* **1996**, *271*, 1698−1702. (d) Goode, J. G.; Hofstein, J. D.; Johnson, P. M. *J. Chem. Phys.* **1997**, *107*, 1703−1716.

(23) (a) Cossart-Magos, C.; Cossart, D.; Leach, S. *Chem. Phys.* **1979**, *41*, 345−362. (b) Cossart-Magos, C.; Cossart, D.; Leach, S. *Chem. Phys.* **1979**, *41*, 363−372. (c) Cossart-Magos, C.; Leach, S. *Chem. Phys.* **1980**, *48*, 329−348. (d) Cossart-Magos, C.; Leach, S. *Chem. Phys.* **1980**, *48*, 349−358. (e) Sears, T.; Miller, T. A.; Bondybey, V. E. *J. Chem. Phys.* **1980**, *72*, 6070−6080. (f) Sears, T.; Miller, T. A.; Bondybey, V. E. *Discuss. Faraday Soc.* **1981**, *71*, 175−180. (g) Sears, T.; Miller, T. A.; Bondybey, V. E. *J. Chem. Phys.* **1981**, *74*, 3240−3248.

(24) (a) Cossart-Magos, C.; Cossart, D.; Leach, S.; Maier, J. P.; Misev, L. *J. Chem. Phys.* **1983**, *78*, 3673−3687. (b) Yu, L.; Foster, S. C.; Williamson, J. M.; Miller, T. A. *J. Chem. Phys.* **1990**, *92*, 5794−5800.

(25) (a) Child, M. S.; Strauss, H. L. *J. Chem. Phys.* **1965**, *42*, 2283−2292. (b) Douglas, A. E. *Discuss. Faraday Soc.* **1963**, *35*, 158−174. (c) Ashfold, M. N. R.; Dixon, R. N.; Stickland, R. J.; Western, C. M. *Chem. Phys. Lett.* **1987**, *138*, 201−208. (d) Ashfold, M. N. R.; Dixon, R. N.; Little, N.; Stickland, R. J.; Western, C. M. *J. Chem. Phys.* **1988**, *89*, 1754−1761. (e) Allen, J. M.; Ashfold, M. N. R.; Stickland, R. J.; Western, C. M. *Mol. Phys.* **1991**, *74*, 49−60.

(26) (a) Herzberg, G.; Hougen, J. T.; Watson, J. K. G. *Can. J. Phys.* **1982**, *60*, 1261−1284. (b) Herzberg, G.; Lew, H.; Sloan, J. J.; Watson, J. K. G. *Can. J. Phys.* **1981**, *59*, 428−440. (c) Herzberg, G.; Watson, J. K. G. *Can. J. Phys.* **1980**, *58*, 1250−1258.

(27) (a) Ohashi, N.; Tsuura, M.; Hougen, J. T. *J. Mol. Spectrosc.* **1995**, *173*, 79−99. (b) Mayer, M.; Cederbaum, L. S.; Koeppel, H. *J. Chem. Phys.* **1996**, *104*, 8932−8942. (c) Ohashi, N.; Tsuura, M.; Hougen, J. T. *J. Mol. Spectrosc.* **1997**, *184*, 22−34. (d) Vituccio, D. T.; Golonzka, O.; Ernst, W. E. *J. Mol. Spectrosc.* **1997**, *184*, 237−249.

(28) (a) Morse, M. D.; Hopkins, J. B.; Langridge-Smith, P. R. R.; Smalley, R. E. *J. Chem. Phys.* **1983**, *79*, 5316−5328. (b) Crumley, W. H.; Hayden, J. S.; Gole, J. L. *J. Chem. Phys.* **1986**, *84*, 5250−5261. (c) Rohlfing, E. A.; Valentini, J. J. *Chem. Phys. Lett.* **1986**, *126*, 113−118. (d) Truhlar, D. G.; Thompson, T. C.; Mead, C. A. *Chem. Phys. Lett.* **1986**, *127*, 287−291. (e) Zwanziger, J. W.; Whetten, R. L.; Grant, E. R. *J. Phys. Chem.* **1986**, *90*, 3298−3301. (f) Morse, M. D. *Chem. Phys. Lett.* **1987**, *133*, 8−13.

(29) (a) Cheng, P. Y.; Duncan, M. A. *Chem. Phys. Lett.* **1988**, *152*, 341−346. (b) Ellis, A. M.; Robles, E. S. J.; Miller, T. A. *Chem. Phys. Lett.* **1993**, *201*, 132−140. (c) Wedum, E. E.; Grant, E. R.; Cheng, P. Y.; Willey, K. F.; Duncan, M. A. *J. Chem. Phys.* **1994**, *100*, 6312−6317.

(30) Bishea, G. A.; Morse, M. D. *J. Chem. Phys.* **1991**, *95*, 8779−8792.

(31) Atanasov, M. *Z. Phys. Chem.* **1997**, *200*, 57−68.

(32) Borden, W. T.; Davidson, E. R. *Acc. Chem. Res.* **1996**, *29*, 67−75.

(33) (a) Poppinger, D.; Radom, L.; Vincent, M. A. *Chem. Phys.* **1977**, *23*, 437−442. (b) Davidson, E. R.; Borden, W. T. *J. Chem. Phys.* **1977**, *67*, 2191−2195.

(34) (a) Roeselová, M.; Bally, T.; Junkwirth, P.; Cársky, P. *Chem. Phys. Lett.* **1995**, *234*, 395−404. (b) Borden, W. T.; Davidson, E. R.; Feller, D. *J. Am. Chem. Soc.* **1981**, *103*, 5725−5729.

(35) (a) Ha, T.-K.; Meyer, R.; Günthard, H. H. *Chem. Phys. Lett.* **1980**, *69*, 510−513. (b) Meyer, R.; Graf, F.; Ha, T.-K.; Günthard, H. H. *Chem. Phys. Lett.* **1979**, *66*, 65−71. (c) Borden, W. T.; Davidson, E. R. *J. Am. Chem. Soc.* **1979**, *101*, 3771−3775.

(36) Raghavachari, K.; Haddon, R. C.; Miller, T. A.; Bondybey, V. E. *J. Chem. Phys.* **1983**, *79*, 1387−1395.

(37) Eiding, J.; Schneider, R.; Domcke, W.; Köppel, H.; von Niessen, W. *Chem. Phys. Lett.* **1991**, *177*, 345−351.

(38) (a) Köppel, H.; Cederbaum, L. S. *J. Chem. Phys.* **1988**, *89*, 2023−2040. (b) Kato, H.; Hirao, K.; Sano, M. *THEOCHEM* **1983**, *13*, 489−494.

(39) Yashizawa, K.; Kato, T.; Yamabe, T. *J. Chem. Phys.* **1998**, *108*, 7637−7644.

(40) Hinde, A. L.; Poppinger, D.; Radom, L. *J. Am. Chem. Soc.* **1978**, *100*, 4681−4685.

(41) Lee, E. P. F.; Wright, T. G. *J. Phys. Chem. A* **1998**, *102*, 4007−4013.

(42) Bally, T.; Truttmann, L.; Williams, F.; Dai, S. *J. Am. Chem. Soc.* **1995**, *117*, 7916−7922.

(43) (a) Davidson, E. R.; Borden, W. T. *J. Am. Chem. Soc.* **1977**, *99*, 2053−2060. (b) Davidson, E. R.; Borden, W. T. *J. Chem. Phys.* **1976**, *64*, 663−666. (c) Borden, W. T. *J. Am. Chem. Soc.* **1976**, *98*, 2695−2700.

(44) Dixon, R. N. *Mol. Phys.* **1971**, *20*, 113−126.

(45) De la Vega, J. M.; Garcia, J. M.; Rico, J. F.; Paniagua, M.; Fernandez-Alonso, J. I. *THEOCHEM* **1983**, *14*, 31−36.

(46) Knight, L. B.; Steadman, J.; Feller, D.; Davidson, E. R. *J. Am. Chem. Soc.* **1984**, *106*, 3700−3701.

(47) (a) Garc'ia de la Vega, J. M.; San Fabiaıan, E. *Chem. Phys.* **1991**, *151*, 335−341. (b) Beärda, R. A.; Wiersinga, H. R. R.; Aarts, J. F. M.; Mulder, J. J. C. *Chem. Phys.* **1989**, *137*, 157−164.

(48) Garc′ia de la Vega, J. M.; Mena, E.; Miguel, B.; San Fabiaan, E. *J. Phys. Chem.* **1995**, *99*, 12135−12140.

(49) (a) Kudo, T.; Nagase, S. *Chem. Phys.* **1988**, *122*, 233−245. (b) Fernandez, J.; Teichteil, C.; Dargelos, A. *Chem. Phys.* **1987**, *114*, 201−207. (c) Fernandez, J.; Arriau, J.; Dargelos, A. *Chem. Phys.* **1985**, *94*, 397−405. (d) Kudo, T.; Nagase, S. *Chem. Phys. Lett.* **1989**, *156*, 289−295. (e) Caballol, R.; Catalá, J. A.; Problet, J. M. *Chem. Phys. Lett.* **1986**, *130*, 278−284.

(50) Cardy, H.; Liotard, D.; Dargelos, A.; Marinelli, F.; Roche, M. *Chem. Phys.* **1988**, *123*, 73−83.

(51) (a) Bent, G. D.; Adams, G. F.; Bartram, R. H.; Purvis, G. D.; Bartlett, R. J. *J. Chem. Phys.* **1982**, *76*, 4144−4156. (b) Bent, G. D. *J. Chem. Phys.* **1994**, *100*, 8219−8232. (c) Bent, G. D.; Bertram, R. H.; Rossi, A. *Mol. Phys.* **1984**, *51*, 1487−1491. (d) Momose, T.; Nakatsuji, H.; Shida, T. *J. Chem. Phys.* **1988**, *89*, 4185−4192. (e) Colwell, S. M.; Amos, R. D.; Handy, N. C. *Chem. Phys. Lett.* **1984**, *109*, 525−531. (f) Benassi, R.; Taddei, F. *Tetrahedron* **1994**, *50*, 4795−4810.

(52) Carter, J. T.; Cook, D. B. *Theochem* **1991**, *83*, 111−122.

(53) (a) Francisco, J. S.; Williams, I. H. *Chem. Phys. Lett.* **1984**, *110*, 240−246. (b) Franciscio, J. S.; Li, Z.; Williams, I. H. *Chem. Phys. Lett.* **1987**, *140*, 531−536. (c) Francisco, J. S.; Li, Z.; Williams, I. H. *Chem. Phys. Lett.* **1991**, *186*, 343−345. (d) Wallington, T. J.; Hurley, M. D.; Schneider, W. F.; Sehested, J.; Nielsen, O. J. *J. Phys. Chem.* **1993**, *97*, 7606−7611. (e) Schneider, W. F.; Wallington, T. J. *J. Phys. Chem.* **1993**, *97*, 12783−12788. (f) Schneider, W. F.; Wallington, T. J. *J. Phys. Chem.* **1994**, *98*, 7448−7451. (g) Bock, C. W.; Trachtman, M.; Niki, H.; Mains, G. J. *J. Phys. Chem.* **1994**, *98*, 7976−7980.

(54) (a) Solomonik, V. G.; Sliznev, V. V.; Balabanov, N. B. *Z. Phys. Chem.* **1997**, *200*, 77−82. (b) Vanquickenborne, L. G.; Vinckier, A. E.; Pierloot, K. *Inorg. Chem.* **1996**, *35*, 1305−1309. (c) Hargittai, M.; Réffy, B.; Kolonits, M.; Marsden, C. J.; Heully, J.-L. *J. Am. Chem. Soc.* **1997**, *119*, 9042−9048.

(55) Bruyndonckx, R.; Daul, C.; Manoharan, P. T.; Deiss, E. *Inorg. Chem.* **1997**, *36*, 4251−4256.

(56) Hehre, W. J.; Radom, L.; v. R. Schleyer, P.; Pople, J. A. *Ab initio Molecular Orbital Theory*; Wiley: 1986.

(57) Pople, J. A.; Scott, A. P.; Wong, M. W.; Radom, L. *Isr. J. Chem.* **1993**, *33*, 345−350.

(58) (a) Pople, J. A.; Head-Gordon, M.; Fox, D. J.; Raghavachari, K.; Curtiss, L. A. *J. Chem. Phys.* **1989**, *90*, 5622−5629. (b) Curtiss, L. A.; Jones, C.; Trucks, G. W.; Raghavachari, K.; Pople, J. A. *J. Chem. Phys.* **1990**, *93*, 2537−2545.

(59) (a) Curtiss, L. A.; Raghavachari, K.; Trucks, G. W.; Pople, J. A. *J. Chem. Phys.* **1991**, *94*, 7221−7230. (b) Curtiss, L. A.; McGrath, M. P.; Baludeau, J.-P.; Davis, N. E.; Radom, L.; Binning, R. J., Jr. *J. Chem. Phys.* **1995**, *103*, 6104−6113. (c) Blaudeau, J.-P.; McGrath, M. P.; Curtiss, L. A.; Radom, L. *J. Chem. Phys.* **1997**, *107*, 5016−5021. (d) Redfern, P. C.; Baludeau, J.-P.; Curtiss, L. A. *J. Phys. Chem. A* **1997**, *101*, 8701−8705.

(60) Curtiss, L. A.; Raghavachari, K.; Pople, J. A. *J. Chem. Phys.* **1993**, *98*, 1293−1298.

(61) (a) Nyden, M. R.; Petersson, G. A. *J. Chem. Phys.* **1981**, *75*, 1843−1862. (b) Petersson, G. A.; Al-Laham, M. A. *J. Chem. Phys.* **1991**, *94*, 6081−6090. (c) Petersson, G. A.; Tensfeldt, T. G.; Montgomery, J. A., Jr. *J. Chem. Phys.* **1991**, *94*, 6091−6101. (d) Montgomery, J. A.; Ochterski, J. W.; Petersson, G. A. *J. Chem. Phys.* **1994**, *101*, 5900−5909. (e) Ochterski, J. W.; Petersson, G. A.; Montgomery, J. A., Jr. *J. Chem. Phys.* **1996**, *104*, 2598−2619.

(62) Chalasinski, G.; Szczesniak, M. M. *Chem. Rev.* **1994**, *94*, 1723−1765.

(63) Herzberg, G. *Molecular Spectra and Molecular Structure*; van Nostrand Reinhold: New York, 1966; Vol. 3.

(64) Chau, F. T.; Karlsson, L. *Phys. Scripta* **1977**, *16*, 258−267.

(65) Liehr, A. D. *J. Phys. Chem.* **1963**, *67*, 389−471.

(66) Hougen, J. T. In *Interactions Among Electronic, Vibrational, and Rotational Motions*. Henderson, D., Ed.; Academic Press: 1970; Chapter 7, pp 307−348.

(67) Child, M. S.; Longuet-Higgins, H. C. *Proc. R. Soc.* **1961**, *245A*, 259−294.

(68) Bernstein, E. R.; Webb, J. D. *Mol. Phys.* **1978**, *4*, 1113−1118.

(69) von Neunann, J.; Wigner, E. *Z. Phys.* **1929**, *30*, 467.

(70) Atchity, G. J.; Xantheas, S. S.; Ruedenberg, K. *J. Chem. Phys.* **1991**, *95*, 1862−1876.

(71) Michl, J.; Bonačić-Koutecký, V. *Electronic Aspects of Organic Photochemistry*; Wiley: New York, 1990.

(72) Herzberg, G.; Longuet-Higgins, H. C. *Trans. Faraday Soc.* **1963**, *35*, 77.

(73) Mead, C. A.; Truhlar, D. G. *J. Chem. Phys.* **1985**, *70*, 2284−2296.

(74) Yarkony, D. R. *J. Chem. Phys.* **1990**, *92*, 2457−2463.

(75) Yarkony, D. R. *Acc. Chem. Res.* **1998**, *31*, 511−518.

(76) For symmetric top molecules with a C_4 axis, the Jahn−Teller active modes will be singly degenerate and a slightly different formalism is required.[68,84−86] The triply degenerate modes of the cubic groups also require a slight extension of this argument.

(77) The dynamic Jahn−Teller effect is sometimes defined as occurring when $D < 1$ (see section 3 for the definition of D). However, since delocalization of the molecule between different asymmetric minima can still occur for $D > 1$, e.g., pseudorotation about the moat in Figure 1, we apply a somewhat loosened definition of "static" and "dynamic" in this paper.

(78) Unfortunately, "pseudo-Jahn−Teller coupling" has often been referred to as "second-order Jahn−Teller coupling." In our usage, "second-order Jahn−Teller coupling" and "quadratic Jahn−Teller coupling" are synonymous and refer to Jahn−Teller coupling in a degenerate electronic state involving the square of the vibrational normal mode, whereas "pseudo-Jahn−Teller coupling" is the coupling of two different electronic states via a vibrational coordinate to the first power.

(79) Bearpark, M. J.; Robb, M. A.; Schlegel, H. B. *Chem. Phys. Lett.* **1994**, *223*, 269−274.

(80) Celani, P.; Robb, M. A.; Garavelli, M.; Bernardi, F.; Olivucci, M. *Chem. Phys. Lett.* **1995**, *243*, 1−8.

(81) Olivucci, M.; Ragazos, I. N.; Bernardi, F.; Robb, M. A. *J. Am. Chem. Soc.* **1993**, *115*, 3710−3721.

(82) Ragazos, I. N.; Robb, M. A.; Bernardi, F.; Olivucci, M. *Chem. Phys. Lett.* **1992**, *197*, 217−223.

(83) Ballhausen, C. J. *Theor. Chim. Acta* **1965**, *3*, 368−374.

(84) Hougen, J. T. *J. Mol. Spectrosc.* **1964**, *13*, 149−167.

(85) Child, M. S. *Mol. Phys.* **1960**, *3*, 601−603.

(86) Moffitt, W.; Thorson, W. *Phys. Rev.* **1957**, *108*, 1251−1255.

(87) Sloane, C. S.; Silbey, R. *J. Chem. Phys.* **1972**, *56*, 6031−6043.

(88) Maslen, P. E.; Handy, N. C.; Amos, R. D.; Jayatilaka, D. *J. Chem. Phys.* **1992**, *97*, 4233−4254.

(89) Barckholtz, T. A. Ph.D. Dissertation, The Ohio State University, 1998.

(90) Barckholtz, T. A.; Applegate, B. E.; Miller, T. A. To be published.

(91) Zhao, K. Ph.D. Dissertation, The Ohio State University, 1996.

(92) Hess, B. A.; Marian, C. M.; Peyerimhoff, S. D. *Adv. Ser. Phys. Chem.* **1995**, *2*, 152−277.

(93) Kaltsoyannis, N. *J. Chem. Soc., Dalton Trans.* **1997**, 1−11.

(94) Pepper, M.; Bursten, B. E. *Chem. Rev.* **1991**, *91*, 719−741.

(95) Balasubramanian, K.; Pitzer, K. S. *Adv. Chem. Phys.* **1987**, *67*, 287−319.

(96) (a) Koseki, S.; Gordon, M. S.; Schmidt, M. W.; Matsunaga, N. *J. Phys. Chem.* **1995**, *99*, 12764−12772. (b) Szalay, P. G.; Baludeau, J.-P. *J. Chem. Phys.* **1997**, *106*, 436−437. (c) Visscher, L.; Lee, T. J.; Dyall, K. G. *J. Chem. Phys.* **1996**, *105*, 8769−8776.

(97) Matsika, S.; Pitzer, R. M. *J. Phys. Chem. A* **1998**, *102*, 1652−1656.

(98) (a) Bernardi, F.; Olivucci, M.; Ragazos, I. N.; Robb, M. A. *J. Am. Chem. Soc.* **1992**, *114*, 8211−8220. (b) Celani, P.; Ottani, S.; Olivucci, M.; Bernardi, F.; Robb, M. A. *J. Am. Chem. Soc.* **1994**, *116*, 10141−10151. (c) Celani, P.; Bernardi, F.; Olivucci, M.; Robb, M. A. *J. Am. Chem. Soc.* **1997**, *119*, 10815−10820. (d) Garavelli, M.; Celani, P.; Fato, M.; Bearpark, M. J.; Smith, B. R.; Olivucci, M.; Robb, M. A. *J. Phys. Chem. A* **1997**, *101*, 2023−2032.

(99) Bearpark, M. J.; Deumal, M.; Robb, M. A.; Vreven, T.; Yamamoto, N.; Olivucci, M.; Bernardi, F. *J. Am. Chem. Soc.* **1997**, *119*, 709−718.

(100) Hougen, J. T. *J. Mol. Spectrosc.* **1980**, *81*, 73−92.

(101) Watson, J. K. G. *J. Mol. Spectrosc.* **1984**, *103*, 125−146.

(102) Amos, R. D.; Alberts, I. L.; Andrews, J. S.; Colwell, S. M.; Handy, N. C.; Jayatilaka, D.; Knowles, P. J.; Kobayashi, R.; Laidig, K. E.; Laming, G.; Lee, A. M.; Maslen, P. E.; Murray, C. W.; Rice, J. E.; Simandiras, E. D.; Stone, A. J.; Su, M.-D.; Tozer, D. J. *CADPAC 5.2*; 1994.

(103) Frisch, M.; Trucks, G.; Schlegel, H.; Gill, P.; Johnson, B.; Robb, M.; Cheeseman, J.; Kieth, T.; Petersson, G.; Montgomery, J.; Raghavachari, K.; Al-Laham, M.; Zakrzewski, V.; Ortiz, J.; Foresman, J.; Cioslowski, J.; Stefanov, B.; Nanayakkara, A.; Challacombe, M.; Peng, C.; Ayala, P.; Chen, W.; Wong, M.; Andres, J.; Replogle, E.; Gomperts, R.; Martin, R.; Fox, D.; Binkley, J.; Defrees, D.; Baker, J.; Stewart, J.; Head-Gordon, M.; Gonzalez, C.; Pople, J. *Gaussian 94*; Gaussian, Inc.: Pittsburgh, 1995.

(104) (a) Lengsfield, B. H.; Yarkony, D. R. In *State-Selected and State-to-State Ion-Molecule Reaction Dynamics: Theory (Part 2)*; Baer, M., Ng, C.-Y., Eds.; Wiley: New York, 1992; Vol. 82. (b) Yarkony, D. R. In *Modern Electronic Structure Theory*; Yarkony, D. R., Ed.; World Scientific: Singapore, 1995. (c) Yarkony, D. R. *Theor. Chem. Acc.* **1997**, *98*, 197−201.

(105) http://ket.ch.cam.ac.uk/software/cadpac.html.

(106) (a) Curtiss, L. A.; Kock, L. D.; Pople, J. A. *J. Chem. Phys.* **1991**, *95*, 4040−4043. (b) Adams, G. F.; Bartlett, R. J.; Purvis, G. D. *Chem. Phys. Lett.* **1982**, *87*, 311−314. (c) Adams, G. F.; Bent, G. D.; Purvis, G. D.; Bartlett, R. J. *Chem. Phys. Lett.* **1981**, *81*, 461−466. (d) Saebo, S.; Radom, L.; Schaefer, H. F., III. *J. Chem. Phys.* **1983**, *78*, 845−853.

(107) (a) Yarkony, D. R.; Schaefer, H. F.; Rothenberg, S. *J. Am. Chem. Soc.* **1974**, *96*, 656−659. (b) Jackels, C. F. *J. Chem. Phys.* **1982**, *76*, 505−515. (c) Jackels, C. F. *J. Chem. Phys.* **1985**, *82*, 311−322. (d) Cui, Q.; Morokuma, K. *Chem. Phys. Lett.* **1996**, *263*, 54−62.

(108) Liu, X.; Damo, C.; Lin, T.-Y. D.; Foster, S. C.; Misra, P.; Yu, L.; Miller, T. A. *J. Phys. Chem.* **1989**, *93*, 2266−2275.

(109) Hedberg, L.; Mills, I. M. *J. Mol. Spectrosc.* **1993**, *160*, 117−142.